12-2008

Transmission Error Analysis and Avoidance for IEEE 802.15.4 Wireless Sensors on Rotating Structures

Jobin Jacob
Clemson University, jobinjacob@gmail.com

TRANSMISSION ERROR ANALYSIS AND AVOIDANCE FOR IEEE 802.15.4 WIRELESS SENSORS ON ROTATING STRUCTURES

A Thesis
Presented to
the Graduate School of
Clemson University

In Partial Fulfillment
of the Requirements for the Degree
Master of Science
Electrical Engineering

---

by
Jobin Jacob
December 2008

Accepted by:
Dr. Kuang-Ching Wang, Committee Chair
Dr. Harlan Russell
Dr. Yong Huang

ABSTRACT

Wireless sensors are increasingly adopted in manufacturing and vehicular systems for monitoring critical components under continuous operation. Many such components move rapidly and frequently in metallic containments with challenging radio propagation characteristics.

For wireless sensors mounted on rotating structures, previous studies identified an eminent increase in packet transmission errors at higher rotation speeds. Such errors were found to occur at specific locations around the rotating spindle's periphery and such locations depended sensitively on sensor location and surrounding geometry. This thesis presents a systematic study of the expected packet error rates due to such errors, and analytically derives the first transmission error rate for a given system. Simulations done on C++ are used to characterize the error region properties. A transmission error avoidance approach based on on-line error pattern inference and packet transmission time control for IEEE 802.15.4 compatible sensor radios is proposed.

The transmission avoidance scheme has two phases: error identification phase to determine the error characteristics of the system and the operational phase to avoid errors. Simulation studies showed a 50% error reduction and up to 75% throughput increase for a rotation system with four symmetric 4º wide error zones with 100% BER inside the error region and 0% BER outside the error region. Higher throughput gains for higher rate and larger size transmissions were also noticed for this system. Simulations also show that the throughput decreases when the packet size duration is greater than the separation between the error zones

DEDICATION

This thesis is dedicated to my family.

ACKNOWLEDGMENTS

I would like to sincerely thank my advisor, Dr. Kuang-Ching Wang for his guidance, support and motivation without which this thesis would not have been possible. Every meeting with him has been motivational and a learning experience. I am indebted to him for his valuable advice throughout the two years of my research.

I would also like to thank Lei Tang and Dr. Huang for their help and support. I am also grateful to all my friends and colleagues in the wireless department.

TABLE OF CONTENTS

Page

LIST OF TABLES

LIST OF FIGURES

List of Figures (Continued)

Figure Page

List of Figures (Continued)

Figure Page

CHAPTER ONE

INTRODUCTION

Wireless sensors, engineered as miniaturized, low-cost embedded devices with integrated sensing, processing, and radio communication capabilities, have recently gained substantial attention for use in different monitoring applications [1]. Wireless sensors are promising for replacing cables in monitoring systems and enabling flexible sensing over structures that are difficult to monitor with wired sensors [2]. Rotating mechanical structures found in a wide range of mechanical, civil, and aerospace systems are among such hard-to-reach structures with crucial monitoring importance [3-6]. Such structures are mostly found in metallic enclosures that are harsh for radio communications, posing to the industry and research community a number of open challenges such as the frequent transmission errors, low data throughput, unknown system reliability, and effects of varied sensor deployment strategies [7-10].

Rotating mechanical structures, typically built within complexly shaped metallic enclosures, create a challengeable condition for wireless data transmission due to their complex, reflective, and fast changing radio paths. Doppler effect might be introduced into the data transmission due to the high rotation speed. During high speed rotation, the stability of radio hardware, such as the antenna connection, is also crucial to reliable transmission. Altogether, these challenging conditions impose on the sensor radios a significant challenge that far exceeds conventional radio communication systems. By far, studies of rotating wireless sensors have not clearly addressed the issue of data transmission reliability [3-6]. The recent study [6] reported the number of received

packets out of all transmitted packets; yet, it did not measure the number of correctly received packets out of all received packets.

In [11,12] a sensor radio mounted on a rotating spindle in a metal enclosure was studied. In [11], it was concluded that errors during rotation were primarily due to multipath and Doppler effects and caused error bursts spanning multiple consecutive bits. In [12], such errors were found to occur near one specific location around the spindle periphery; its vicinity was referred to as an error region, and a reliable transmission method based on automatic repeat request (ARQ) was introduced to recover transmission errors. *The ARQ approach achieved a high retransmission success rate; nevertheless, new transmissions still faced above 20% packet error rates, severely undermining the achievable data throughput and wasted substantial energy in retransmissions. As later shown in this thesis, packet error rates can easily reach as high as 50% under certain configuration and channel characteristics*. In [13], the temporal distribution and size of error regions were analyzed based on recorded time stamps and bit contents of failed probing transmissions. Probing transmissions were also used to determine the effects on the error distribution with the change in rotation speed of the spindle and clock drift of the sensors.

With multipath and Doppler effects being the primary causes of transmission errors for a rotating sensor, the error region distribution is expected to depend sensitively on the surrounding structure, sensor position, and rotating speed. In [8], the PERs were found to differ substantially by moving the receiver's location by just 3cm. To avoid transmissions that would most probably result in errors, a sensor radio must be aware of

its error region distribution in order to determine its transmission strategy, while obtaining accurate sensor position around the periphery during high speed rotation is very difficult without complex hardware design. To reduce such transmission errors for enhancing data throughput and energy efficiency, an error-avoidant transmission scheme utilizing error region distribution needs to be considered.

The purpose of this thesis is to characterize the error region and its avoidance scheme. An analytical model is developed based upon the protocol of IEEE802.15.4. Different experiments and simulation results are used to evaluate the effectiveness of the proposed transmission error avoidance mechanism. A rotating radio simulator is developed based on the IEEE 802.15.4 protocol to model the radio error model, error distribution inference, and transmission time control. Simulation results are divided according to the two phases of the transmission error avoidance method. In the training phase the sensor utilizes probing packets to generate the error location distribution. This is used to identify the error locations and their widths. In the operational phase the sensor sends data packets. Synchronization is done initially to deduce the location of the transmitter with respect to its error location. Simulation results show a 50% error reduction and up to 75% throughput increase for a rotation system with four symmetric 4º wide error zones with 100% BER inside the error region and 0% BER outside the error region. Higher throughput gains for higher rate and larger size transmissions are also noticed for this system. The main contribution of this thesis is the transmission error analysis method and the transmission error avoidance scheme used for a rotating wireless sensor system.

The rest of the thesis is organized as follows. In chapter 2 the related work and achievements are described. Chapter 3 describes the experimental setup of the wireless sensors in the computer numerical control (CNC) lathe and the IEEE 802.15.4 MAC protocol. The model developed for the rotating error system is described in chapter 4, and the transmission error avoidance scheme is described in chapter 5. The conclusions and future work are discussed in chapter 6.

CHAPTER TWO

BACKGROUND AND RELATED WORK

IEEE 802.15.4 radios are used in networks to ensure low cost communication with low power consumption. The thesis focuses on the communication between an IEEE 802.15.4 radio attached to a rotating device and a stationary radio. In this chapter the current use of IEEE 802.15.4 radios and the constraints faced by radios on fast rotating structures is discussed.

2.1 Current Use of IEEE 802.15.4 Radios

The IEEE 802.15.4 standard compliant radios are designed for low-data-rate, low-power, and short-range transmission [15] in the 868/915 MHz and 2.45 GHz Industrial, Scientific, and Medical (ISM) radio bands. Existing IEEE 802.15.4-compliant radios do not implement complex circuitry such as a RAKE receiver which improves reception in the presence of multipath channels or a carrier frequency tracker for compensating Doppler shifts, but rely on the limited multipath and Doppler tolerance inherent in its direct sequence spread spectrum (DSSS) modulation scheme.

Numerous field measurement studies of wireless sensors have been done, e.g., [16-19]. Most of these studies included IEEE 802.15.4 radios in addition to other sensor platforms with their respective radio protocols, frequency bands and power levels. Measurements were conducted in both indoor and outdoor settings and had the same conclusions that there exists a grey zone [16,18] at a specific distance from the

transmitter, within which the receivers link quality fluctuates with even small displacements. The studies also conclude that link asymmetry occurs, such that a node may be able to transmit to another node but vice-versa may not happen, even if the nodes were set to the same transmit power. In addition to studies on wireless sensor links, work has been done on the use of IEEE 802.15.4 radios in monitoring the environment [20] and location estimation [21-22]. [23] discusses the introduction of an IP stack to the IEEE 802.15.4 stack to enable the efficient transmission of IPv6 datagrams over IEEE 802.15.4 links. This opens up the use of such radios for Internet applications.

The majority of applications examined to-date had sensors deployed on the ground or on structures that are either stationary or slow moving. Very few studies have examined the use of wireless sensors on structures that move substantially within the timeframe of a wireless transmission. Rotating structures, specifically, are commonly found in mechanical and vehicular systems with substantial monitoring importance.

Only few studies have examined wireless sensors operating on a rotating structure. In [2], wireless sensors were installed inside polymer covered cylindrical rolls to measure acoustic emission pulse counts and surface temperatures; up to 10k packets per second data were transmitted over an IEEE 802.11 radio. In [3], a wireless motor spindle measurement system measured torque, power, and rotation speed with sampling rates up to 963.9 Hz, and the data were transmitted over a low-power digital radio at 19200 bits per second (bps). Both studies did not mention transmission errors in their experiments.

2.2 Constraints Faced by Radios on Rotating Structures

Radio communication challenges under moving conditions have been studied extensively in the context of cellular mobile communications. The conclusions of such work cannot be directly applied to the rotation of a wireless sensor. Sensor radios differ greatly from cellular radios in their very low transmit power, simple antenna and circuitry design. Commercial wireless sensors trade off robustness for low costs

Rotating mechanical structures are usually located within confined enclosures, with the structures themselves and their surroundings made of metallic materials. To monitor such rotating structures, a typical wireless measurement system usually consists of two parts: 1) the measuring and transmitting unit, which is mounted on or within the rotating structure, and 2) the receiving unit which is mounted on a stationary part near the rotating structure. Within such an environment, a received radio signal is expected to have rich multipath radio components, each experiencing different path loss and Doppler effect, and resulting multipath effects that depend on the relative phases, amplitudes, and frequency shifts of all transmitted radio components. While wireless sensors have been demonstrated with stably acceptable performance in amicable environments such as in an office or out in the field, the performance of rotating wireless sensors may be severely affected by harsh monitoring environments due to excessive obstruction, multipath propagation, antenna polarization, Doppler shift, and electromagnetic noise.

Radio signal attenuates along the propagated path. The energy attenuation, known as the path loss, is proportional to a certain power of the propagated distance, with additional obstruction and/or refraction loss caused by objects along the path. Signal is

radiated from an antenna in a span of directions regardless of their types. When static or moving objects exist in the surrounding, the radio signal may follow multiple reflected paths to reach a receiver with different amplitudes and phases due to the different path lengths. The received signal is the sum of all such multipath signal components, which generally causes distortion in the signal duration and waveform. Rotating structures also face the additional challenge of the Doppler effect, which occurs due to the fast change of the distance between the transmitting and receiving sensor during signal transmission. The distance change results in frequency shifts and signal duration changes that also distort the received signal [24]. Electromagnetic noise is typically present around engineering systems.

In [11], experiments with rotating wireless sensors concluded: (1) the radio performance was dominated by multipath effects, whereas machine electromagnetic noise and hardware stability effects were insignificant; (2) when stationary, the radio had consistently low PERs; (3) when rotating, PERs increased with speed at some locations but not all; the dependency changed when receiver was moved by 3cm; (4) bit errors occurred in bursts, when the transmitter rotated past a particular location; (5) path loss, antenna directive gains and stability, machine noise, and automatic gain control had insignificant relevance with bit errors.

The experimental setup utilized in this thesis is designed to model the essential features of a wireless sensor-based monitoring platform for rotating structures in civil, mechanical, and aerospace systems. The sensor platform can potentially be integrated with sensors for acoustic emission, strain gauge, thermocouple, accelerometer, etc.

Examples of such applications can be found in roll contact monitoring [3], grinding wheel truing and grinding monitoring [4], and motor shaft torque monitoring [5, 6]. The evaluation study conducted serves to highlight key performance characteristics that cannot be overlooked in designing a reliable wireless monitoring system, whereas the experimental procedure is applicable for channel characterization in a wide range of systems.

CHAPTER THREE

SYSTEM DESCRIPTION

In this chapter the rotating wireless sensor test bed is explained. The experimental results on this test bed form the basis for this thesis. The transmission error avoidance scheme developed utilizes the timing information of the IEEE 802.15.4 MAC protocol. This chapter also explains the MAC protocol and how its packet scheduling can be used in the transmission error avoidance scheme, it also explains the reason for choosing the non-beacon mode version of the protocol for the transmission error avoidance scheme.

3.1 Rotating Wireless Sensor Test Bed

The testbed is built with two wireless sensors mounted inside a computer numerical control (CNC) lathe, with one base station placed outside the machine for issuing commands and retrieving data from the wireless sensors.

Crossbow MicaZ motes [26] are chosen as the wireless sensors for this testbed. The MicaZ mote adopts an IEEE 802.15.4-compliant radio based on the Chipcon CC2420 chip, which supports 250 Kbps raw data rate, controllable transmit power range of -25 dbm to 0 dbm, and 16 channels in the 2.4 GHz ISM band. The radio chip feeds to a quarter-wavelength monopole antenna (about 1.2 inches long) screw-attached to the circuit board with an MMCX connector that is designed for a slot-less, snap-fitting, and minimal-leakage contact. The mote outputs various radio parameters to be used in the

experiments. For each received packet, an 8-bit received signal strength indication (RSSI, linear transformable into dBm unit), an 8-bit link quality indicator (LQI), and the output of a 16-bit cyclic redundancy check (CRC) error-detecting circuit [27] are provided. The radio adopts direct sequence spread spectrum (DSSS) and O-QPSK half-sine modulation, such that each 4-bit data is mapped to a pseudo-random 32-chip binary spreading sequence, which is transmitted with O-QPSK modulation. The mote is 2.25 by 1.25 by 0.25 inch^3 in size.

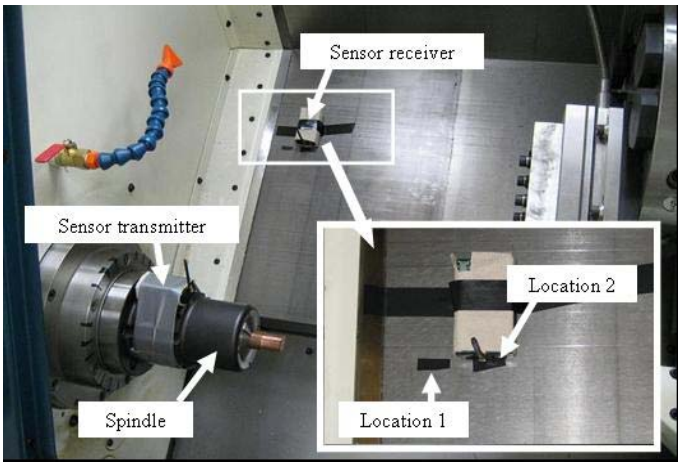

Figure 3.1. Rotating sensor testbed photograph

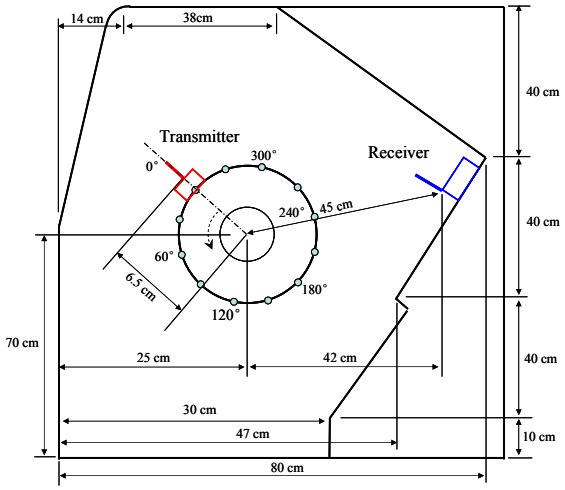

Figure 3.2. Projected view from the right side of the rotating sensor test bed (not to scale)

The machine used in the testbed is the Hardinge Talent 6/45 CNC lathe with a speed-controllable rotating spindle enclosed in a metallic chamber. The spindle can rotate at a maximum speed of 6000 rpm and minimum speed of 60 rpm. Figure 3.1 shows a photograph and Figure 3.2 shows a cross-section view along the spindle axis. The transmitter mote is tape-bound to the spindle surface, with its antenna perpendicular to the surface. The receiver mote is placed on the metallic side board next to the spindle, aligned with the transmitter on the plane perpendicular to the spindle. Transmission experiments are controlled via a base station composed of a MicaZ mote connected to a Crossbow mote interface board (MIB510), located outside the lathe. The precise location of the base station is not relevant, as it only communicates with the sensors for control and data logging between experiments. As illustrated in Figure 3.3, the base station communicates with the sensors over the same IEEE 802.15.4 channel, while it interfaces with a personal computer (PC) for data logging over a universal asynchronous

receiver/transmitter (UART) serial cable.

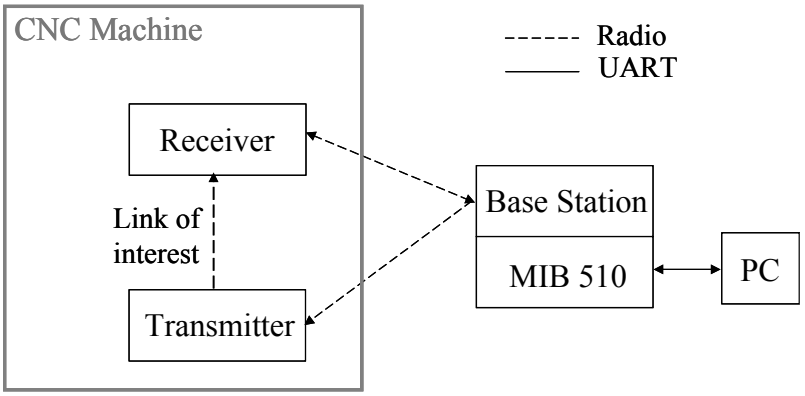

Figure 3.3. Sensor communication architecture.

Wireless transmission experiments are conducted to transmit a sequence of packets using the ARQ reliable transmission method and to record all transmission errors seen at the receiver. With the IEEE 802.15.4 acknowledgement option enabled, the receiver sends a short acknowledgement (ACK) packet to the transmitter immediately after receiving a packet correctly; otherwise, an ACK is not sent and the transmitter will retransmit the packet after one IEEE 802.15.4 ACK timeout duration. The correctness of a packet is determined at the receiver by checking a hardware-generated cyclic redundancy check (CRC) bit. If the CRC bit is 1, the entire packet is considered to have been received correctly. If CRC bit is 0, some bits in the packet must have been corrupted. The bit sequences of all incorrectly received packets are recorded with their received timestamps for further processing. After each successful transmission (transmitter receiving an ACK), the transmitter waits for a standard-defined random backoff duration and proceeds to send the next packet. Effectively, the ARQ approach

sent a continuous flow of packets from the transmitter to the receiver, with short intervals between every two consecutive transmissions. Experimental results are discussed in chapter 4.

3.2 IEEE 802.15.4 MAC Protocol

The proposed transmission error avoidance scheme is based upon the scheduling of the packet transmissions by the 802.15.4 MAC protocol; hence the following section describes the 802.15.4 MAC protocol.

The IEEE 802.15.4 MAC Protocol is essentially a CSMA/CA protocol and can be operated in two different modes [15], namely the beacon mode (slotted CSMA/CA algorithm) and the non-beacon mode (unslotted CSMA/CA algorithm) . Figure 3.4 shows the non-beacon mode of operation. The transmission time of the packet depends on which mode is chosen.

With the beacon mode, a coordinator radio can assign transmission slots to each device radio. The coordinator broadcasts periodic beacons at its chosen interval, between two beacons the coordinator can allocate contention access period (CAP) slots, guaranteed time slots (GTSs), and inactive (low-power sleep) slots. A device radio can transmit a data packet during CAP based on slotted CSMA/CA (carrier sense multiple access with collision avoidance), i.e. waiting a randomly chosen number of idle slots prior to transmission, or it can transmit data packets in its GTS assigned by the coordinator.

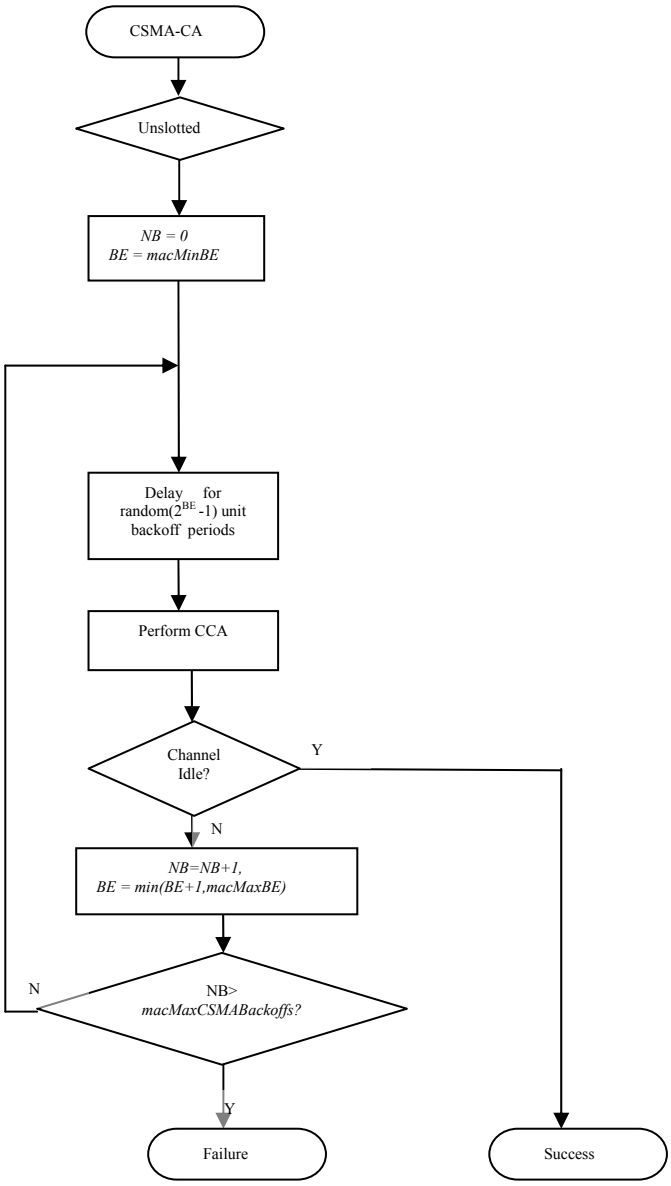

Figure 3.4. Unslotted CSMA/CA algorithm [15]

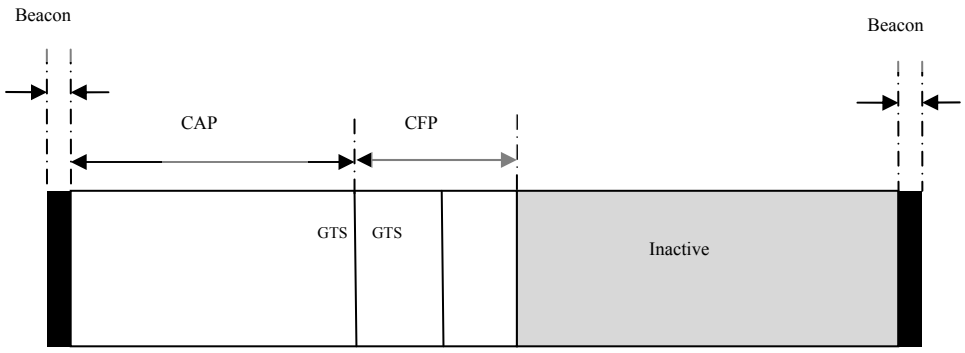

Figure 3.5. Beacon mode frame structure [15]

Conceptually, the proposed approach can be easily implemented with the beacon mode, by configuring the receiving radio as a coordinator, the transmitting radio as a device, the beacon period equal to the rotation period, and assign the device with GTS slots aligned with the low-error regions. In reality, however, the standard imposes various constraints that make it very restrictive, if not impossible, to implement the concept properly with the beacon mode.

These constraints are: (1) a minimum of aMinCapLength symbol duration must be allocated for CAP after each beacon for control frame exchange and new device joins, (2) GTS can only be allocated after CAP, (3) it is not always possible to assign a beacon period equal to the rotation period, (4) beacon frames must be correctly received every period for GTS transmissions to proceed. These constraints result in substantial overheads and scheduling inefficiencies in practice.

With non-beacon mode, there is no distinction between a coordinator and a device radio for transmission purposes. Each radio attempts to transmit a packet using an unslotted CSMA/CA algorithm. The radio waits for one fixed clear channel assessment (CCA) duration and a random number of backoff slots. If the channel remains idle during the wait, the transmission proceeds, and the receiver responds with an ACK if the packet is received correctly. The expected time for completing a data transmission is thus the time from start of CCA till end of ACK reception. The main inefficiency with this approach lies in the random backoff periods. Fortunately, the standard allows setting minimum values for the random backoff parameters to limit the minimum backoff window to 2^0 backoff periods and the maximum backoff window to 2^3 backoff periods. The non-beacon mode approach is considered for the transmission error avoidance with a maximum back-off duration of 1 period, because of all these advantages.

CHAPTER FOUR

ROTATION ERROR MODEL

This chapter focuses on the study of the error patterns of the rotation system which is used later on in developing the error avoidance scheme. The first section of this chapter explains the experimental results which led to the identification of the error region. The second section provides an analytical model for analyzing the packet error rate in such a system and the third section describes the simulation model for the system.

4.1 Experiment Results

ARQ experiments were conducted at 2054 rounds per minute (rpm) rotation with the configuration shown in Figure 3 1. The radio transmitted at -25 dBm power in channel 26 (2478.5 ~ 2481.5 MHz). In each experiment, 5000 packets of packet size 92 bytes (10 byte header size included) were transmitted continuously; the sender was always backlogged and sent a new packet whenever the previous packet had been transmitted/retransmitted successfully or the maximum retry limit (9) was reached.

In each experiment the sender sent probing transmissions of a known pattern (all 1's) and size (100 bytes) at a chosen interval to the receiver. For each packet received with errors (failing CRC check), the receiver recorded the packet's received timestamp and bit contents. Using a sliding window algorithm, the receiver identified all error bursts in these packets; an error burst is defined as a set of consecutive bits with at least a specified fraction H of bits in error. The time interval between the start times of two

consecutive error bursts, T_i, was measured to derive the normalized error burst distance which is defined below.

Definition 1: Error Burst Distance Distribution

Consider N consecutive error bursts obtained from the probe packets. Let the time interval between the start times of the i^{th} and $i+1^{th}$ error bursts be T_i, the normalized error burst distance D_i for the i^{th} error burst is defined as

$$D_i = \frac{T_i \text{ modulo } T_R}{T_R} \qquad (1)$$

were T_R is the spindle rotation period. The normalized error burst distance represents the distance (in fraction of periphery) between the two positions on the periphery where consecutive error bursts have occurred.

Figure. 4.1 shows the error burst distance distribution estimated on the rotating wireless sensor testbed. With the two main modes residing near 0 and 1, respectively, it meant that the errors had always occurred in the same vicinity, which was defined as an error region. The error burst distance distribution is considered mainly because of the clock drift error seen in the sensors. Another parameter called error burst location distribution which is explained in Section 5.1 is used in determining the error patterns if the sensor clock drift error is overcome. Further discussion on sensor clock drift is given in Section 5.1.

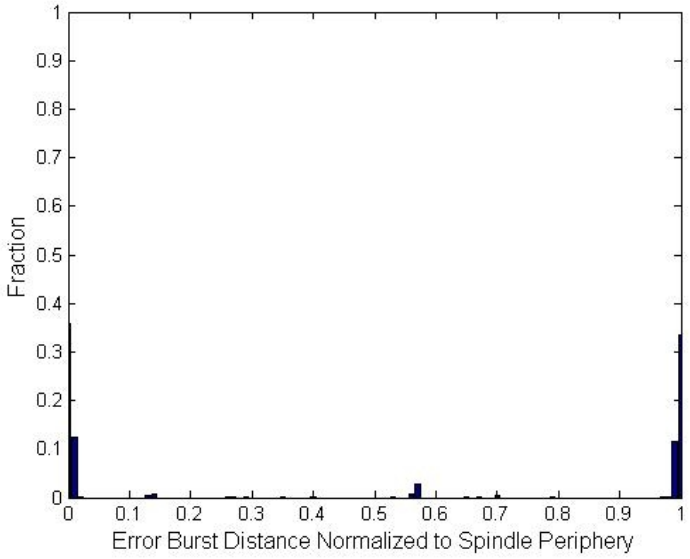

Figure 4.1. Normalized error burst distance distribution from testbed experiments at 2054 rpm with 5000 packets sent at 15 msec fixed intervals

ARQ experiments were also conducted with packets of chosen packet size (30, 60 and 92 bytes) transmitted at chosen constant interval (0, 100, 150, and 200 msec) for a constant rotation speed of 2000rpm. The results of the experiment are shown in Table 4.1. First transmission rate gives the percentage of packets received with error during their first transmission, while retransmission count gives the number of retransmissions required for the successful delivery of the packet. The table shows that the first transmission error rate increases with packet size and the average retransmission count is nearly one. This shows that almost all retransmissions are successful and indicates that the retransmissions always tend to happen in a “low- error” region.

Table 4.1. First transmission error rate and mean of retransmission count vs packet size at different packet generation interval**.**

Packet Generation Interval = 0 msec				**Packet Generation Interval = 100 msec**		
Packet size	**1st trans. error rate**	**Retrans. count mean /standard deviation**		**Packet size**	**1st trans. error rate**	**Retrans. count mean /standard deviation**
30 bytes	0.098	1.026/0.159		30 bytes	0.067	1.000/0.000
40 bytes	0.137	1.253/0.435		60 bytes	0.136	1.000/0.000
92 bytes	0.151	1.191/0.424		92 bytes	0.171	1.140/0.365
Packet Generation Interval = 150 msec				**Packet Generation Interval = 200 msec**		
30 bytes	0.059	1.000/0.000		30 bytes	0.067	1.000/0.000
60 bytes	0.143	1.000/0.000		60 bytes	0.087	1.046/0.209
92 bytes	0.181	1.042/0.202		92 bytes	0.220	1.112/0.316

4.2 Proposed Error Model

The error burst distribution indicated that at a certain rotation speed one or a few "high-error regions" can be identified, and among them are interleaving "low-error" regions. Figure 4.1 indicates that errors tend to occur at the same position which could mean that the system could have just one error region. If any segment of a packet is transmitted during the high-error region, those bits have a greater possibility to have errors; on the other hand, any segment transmitted in a low-error region is expected to see less, if any, error bits in it. A different system with more multipath and Doppler effects could result in a different number of error regions; but all systems can be represented by the same error model.

To determine the error model, probe packets are sent. The bits of the probing packets are analyzed to determine all the possible error bursts and the error burst distance distribution is generated using the start times of the error burst.

Let M be the number of distinguishable error regions identified from the error burst distance distribution. Each error region will have its own width W_i which is determined by the bit error rate H_i inside the error region. The bit error rate inside the error region would be higher than the bit error rates in the remaining "low-error regions". The position of each error region can be identified by its center C_i which is represented in degrees. Thus each region of the system can be represented by the parameters $\{ W_i, H_i, C_i \}$ where $i = 1,2,\ldots, M$.

An example of a three error zone system is shown in Figure 4.2

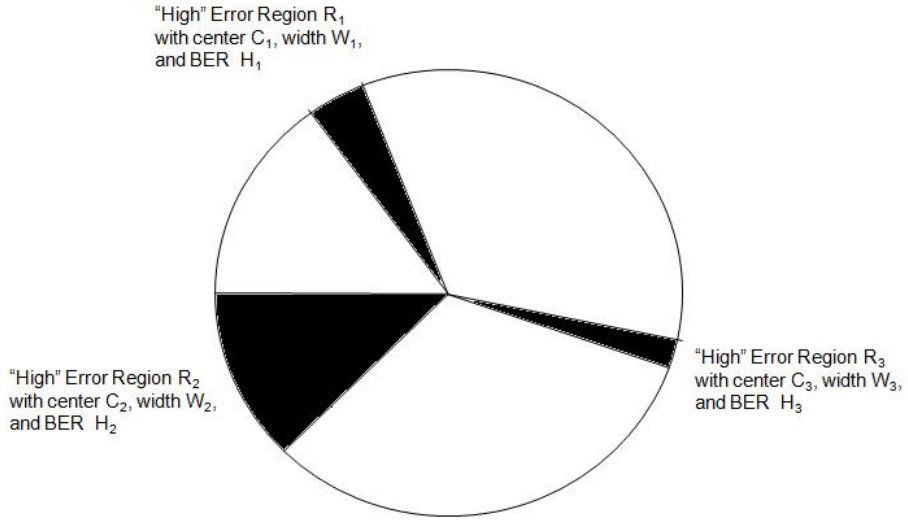

Figure 4.2. Three error region pattern

To extract the model parameters from actual experimental data a sliding window algorithm is adopted.

The sliding window algorithm is defined as follows. Given the bit sequence of an incorrectly received packet of size N bits, $\{S_i, i=1\ldots N\}$, a subset of consecutive bits in $\{S_i\}$ is defined as a window $W(j, l)$ where j indicates the sequence number of the first bit in $W(j, l)$ and l is the number of bits in $W(j, l)$. The algorithm initiates with j=1 (the first bit), l=2 (two bits in the window), and a specified error rate threshold H. The error rate for $W(j, l)$, P_W, is defined as the number of error bits in $W(j, l)$ divided by the total number of bits in $W(j, l)$. In each step, if P_W is less than H, j increases by one (the window shifts by one bit position); otherwise, l increases by one. One round is considered completed when the window encloses S_N, and another round is started with j=1 and the l value as at the end of the previous round. The algorithm repeats until l does not increase in one round; thus, l is the size of the largest window that exceeds the specified error rate threshold, and it is used to estimate the size of the error region.

The sliding window algorithm was applied to all error packets in the ARQ transmission experiments. With different threshold H, the error burst window size for all error packets are found. The error packets have a size of 92 bytes. The maximum, mean, and standard deviation of the window sizes are summarized in Table 4.2. Each (H, l) pair provides a valid model to reproduce the observed error statistics. With l given in bits, the corresponding error region width can be calculated in terms of the duration or the rotated angle given the rotation speed. Note that IEEE 802.15.4 radios have a data rate of 250 kbps; thus l bits represent a duration of l/(250k) sec. . The statistics show that the error

region size and the transmission error rate are inter-dependent. The table shows that the mean error width decreases with increase in the error burst threshold. The table also shows that the mean error width size is between 4 and 23 bits which is equivalent to 0.2 to 1.1 degrees at a rotation speed of 2054 rpm. Thus all simulations consider an error region width of 4 degrees which is a close approximation to the width calculated using the sliding window algorithm. Such a small error region can cause an average PER of 11.8% without the ACK option enabled. As will be shown with simulation in Section 5.1, the PER can increase substantially with even a few more such narrow error regions. With four error regions (4 degree wide, evenly spaced), the PER can be as high as 50%.

Table 4.2. Maximum, mean, and standard deviation of detected error window sizes with varied error rate thresholds.

H	***Max l (bits)***	***Mean l (bits)***	***Std.Dev (bits)***
0.4	215	23.0	25.0
0.5	149	16.5	18.0
0.6	81	11.0	12.0
0.7	67	7.3	8.0
0.8	52	5.2	5.0
0.9	28	4.0	2.8

It is the highly predictable error region distribution and the high PER that can be caused by very small error regions that have motivated this thesis to study means to avoid such errors over existing sensor radios by controlling packet transmission times based on

identified error region distribution. Equation 1 on page 20 shows that the error burst distance distribution is readily obtainable with accurate knowledge of the rotation speed and times of previously seen error bursts. Obtaining such information and ensuring its accuracy are by themselves challenging, since (1) accurate rotation speed can be obtained only with complex sensor design or has to be reported by the rotating machine, (2) the estimated or reported rotation speed can still be inaccurate, and (3) the sensor clock can be inaccurate with respect to the clock used for speed measurement. In section 4.3.3, the impact of inaccurate knowledge of rotation speed is studied.

4.3 Error Rate Analysis

As explained in section 3.2, for error avoidance the IEEE 802.15.4 MAC protocol version considered for this thesis is the CSMA/CA non-beacon mode version. Our system comprises just one sensor communicating to the other sensor at a time and hence the channel is always idle for transmitting data and there is no chance of collisions. Understanding the MAC protocol packet scheduling time in this system is easy and can be utilized to determine the error rate in the system. So this section explains the parameters of the CSMA/CA algorithm involved in scheduling the packet transmission and comes up with intuitive and numerical analysis to determine the error rate.

As shown in Fig. 4.3, every transmission is preceded by a random back-off time δ and a clear channel access (CCA) duration. The maximum back-off time is Δ which corresponds to 1 random back-off period. There is an additional turnaround time D involved for switching the radio from receiver mode to transmit mode or vice versa. If the

link layer ACK option is enabled an acknowledgement packet is sent for every correctly received packet. Our experimental results in Chapter 3 show that the retransmission success rate is high and indicates the effectiveness of using an ARQ algorithm for retransmission of incorrectly received packets and hence the ACK option is enabled. Thus every incorrect packet is retransmitted after a constant acknowledgement time out duration τ. A picture showing the time spent in transmission of a correct packet and a packet with erorrs is shown in Fig. 4.3 and 4.4.

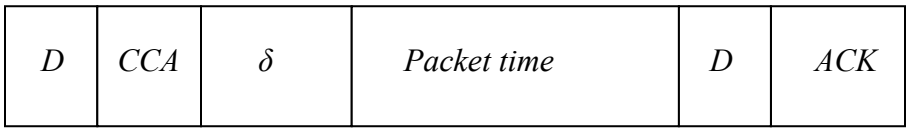

Figure 4.3. Illustration of the time taken in transmitting a correct packet (Timings not to scale)

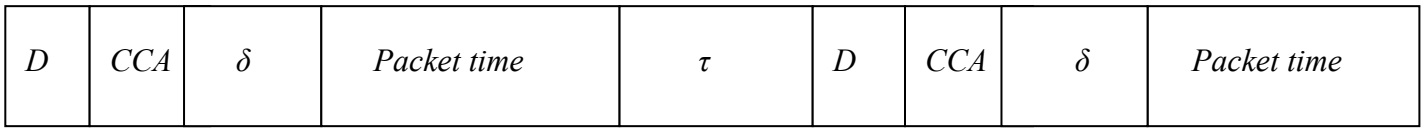

Figure 4.4. Illustration of the time taken in transmitting an incorrectly received packet and the corresponding retransmission (Timings not to scale)

4.3.1 Qualitative Interpretation of PER Dependency on Rotation Speed

Packet error rate (PER) is defined as the fraction of the transmissions that are successful with the ACK option enabled. For a three error region distribution with error zones centered at 0, 120 and 240 degrees and error regions width of 4 degrees each, the expected PER can be found analytically with respect to the temporal pattern and size of the transmitted packets. The analysis provided in this section gives an intuitive

explanation for the dependence of PER on rotation speed based upon three different assumptions. The explanation given is only corresponding to the given symmetric error system.

Assumption 1: Considering only the packet transmission time in the IEEE 802.15.4 MAC Protocol.

Consider a rotation cycle with a given error region distribution as illustrated in Figure 4.5. During the time a *B*-byte packet is transmitted at rate *R* bits per second, a sensor traverses for $8Bw/R$ degrees around the circumference of a spindle rotating at speed *w*; if the traversed region overlaps the error region in any part, the packet may contain a number of error bits. To simplify the analysis, a 100% BER within an error region, 0% BER outside an error region, and no error corrections are considered.

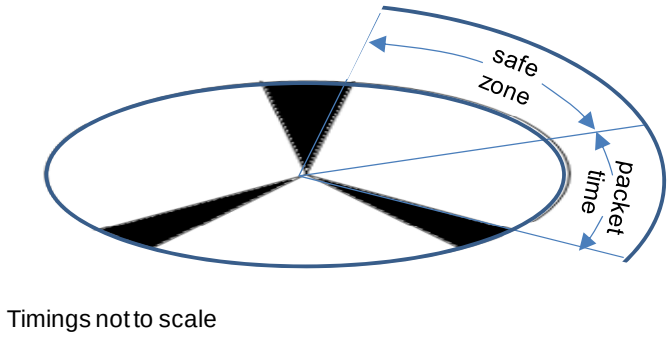

Figure 4.5. First safe zone illustration considering traversed range during a packet time only. While not shown, the same rule applies for the rest of the cycle

The transmission correctness depends on the starting location of a packet. Let any portion around the circumference that a packet can start and end its transmission without

encountering an error region be called a safe zone. The wider the safe zone, the more probable a packet initiated at random time can complete successfully. If the pre-transmission wait times required by the IEEE 802.15.4 protocol is ignored for a given error distribution, the safe zone depends on the traversed degrees during one packet time, which is proportional to the rotation speed. The faster the rotation speed, the more degrees a sensor traverses during its transmission, and hence the smaller safe zone it has. The reasoning suggests an increasing chance of packet errors with increasing rotation speeds if packets are transmitted at arbitrary times without an error avoidance mechanism; the phenomena was observed in actual experiments .

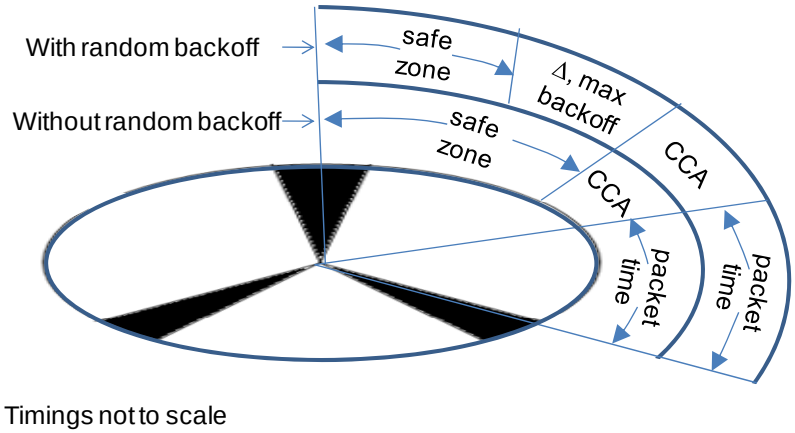

Figure 4.6. Safe zone illustration considering traversed range in CCA and packet time, with and without random backoff. While not shown, the same rule applies for the rest of the cycle.

Assumption 2: Considering the CCA and random back-off time of the IEEE 802.15.4 MAC Protocol.

In reality, an IEEE 802.15.4 sensor node in the non-beacon mode must wait for a constant clear-channel-assessment (CCA) duration and a random back-off duration prior to transmitting a packet. This variable pre-transmission wait changes the start time analysis slightly as illustrated in Figure.4.6. Here the distance travelled in the CCA duration is assumed to be less than the error region width. Hence the constant CCA duration simply shifts the safe zones ahead but does not change the overall safe zone size and, therefore, does not change the PER. The random back-off duration, however, can reduce the safe zone size. As the figure shows, the total safe zone decreases when the wait time increases from CCA to CCA+Δ, where Δ stands for the maximum backoff duration. This is because the safe zone accounts for the areas where a data transmission can begin and be sure to complete entirely outside any error region and a transmission with maximum random back-off duration would need to start at a position earlier than without random back-off. This would result in pushing the boundary of the safe zone further back. Outside the safe zone, there are some areas where a transmission can begin and has some less than 100% probability to complete outside an error region depending on its random backoff duration.

Assumption 3: Considering the ACK time of the IEEE 802.15.4 MAC Protocol.

The link layer ACK option of IEEE 802.15.4, if enabled, requires a radio *A* that receives a transmission correctly to transmit an ACK packet back to the sender, say radio

B, of that transmission. If *B* happens to be in an error region, it will not receive the ACK correctly and the transmission will be considered a failure. For reliability sensitive applications, the ACK option is expected to be indispensable and the ACK failure conditions would affect the resulting PER performance. An ACK is transmitted at a transmit-receive-turnaround time *D* after the completion of the data packet transmission. The impact of ACKs on PER is not as obvious as that of data packets. Given a correct data transmission taking place outside an error region, its ACK must also start and end without crossing an error region for the data transmission to successfully complete. Hence, the safe zone must be redefined as the areas where a data transmission can begin such that it and its corresponding ACK will both complete outside any error region.

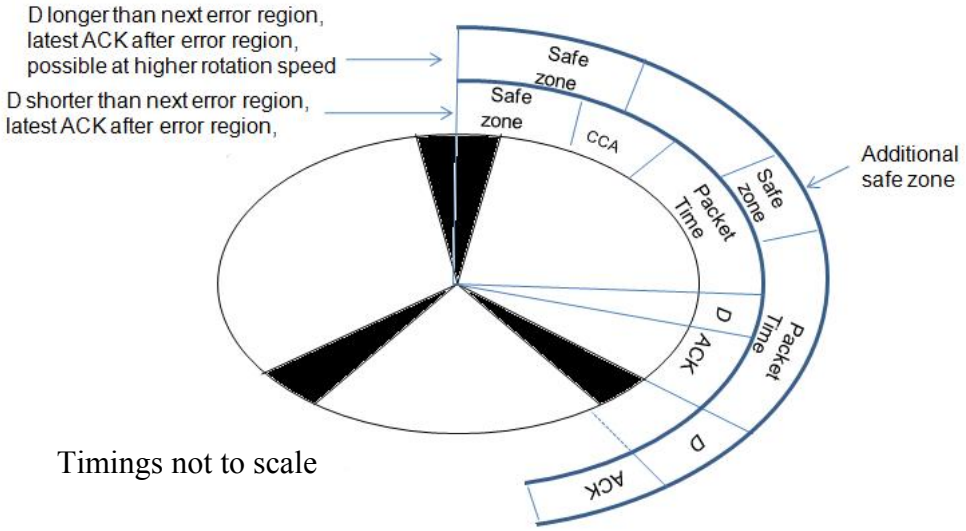

Figure 4.7. Safe zone illustration considering traversed range during CCA, packet time, turn-around time, and ACK time, without random backoff. While not shown, the same rule applies for the rest of the cycle.

It can be shown that the safe zone with ACKs considered is either less than or equal to the safe zone estimated without ACKs. As illustrated in Figure 4.7, the safe zone size depends on the relative sizes of the turn-around time *D* and the subsequent error region size after a data transmission. There are two cases shown in Figure 4.7. If the traversed range during *D* is shorter than the following error region size, the ACK must take place before the error region and thereby reduce the available safe zone size. The range traversed during *D,* CCA, ACK or packet time depends on the rotation speed and greater the rotation speed larger would be the range traversed So if the traversed range during *D* is wider than the following error region size, ACK can potentially take place after the error region and gain an additional safe zone that is equal to the range difference between *D* and the error region size as shown in Figure 4.7. It is thus clear the safe zone size changes with rotation speed, since the traversed range during an ACK time changes accordingly. As the speed increases, the data packet range increases, such that the safe zone decreases, but the *D* range increases as well, such that an additional safe zone appears once *D* range exceeds the error region range; as the speed decreases, the reverse trends apply. Thus, the overall safe zone and, therefore, the resulting PER is not necessarily monotonic with the speed changes. The rotation speed at which the *D* range equals the error region width is the speed at which the change can be noticed. This is speed is calculated from the equation.

$$D*(\text{rotation speed})*6 = \text{Error region width.} \qquad (2)$$

To illustrate the concept, randomized simulations were conducted with our simulator with 92 byte packets and three 4-degree wide error regions centered at 0, 120,

and 240 degrees on the spindle. As shown in Figure. 4.8, the PER generally increased with speed but had an exception decrease past 3500 rpm, after which the increasing trend resumed. Equation (2) when solved for this scenario gives the same result of 3500 rpm.

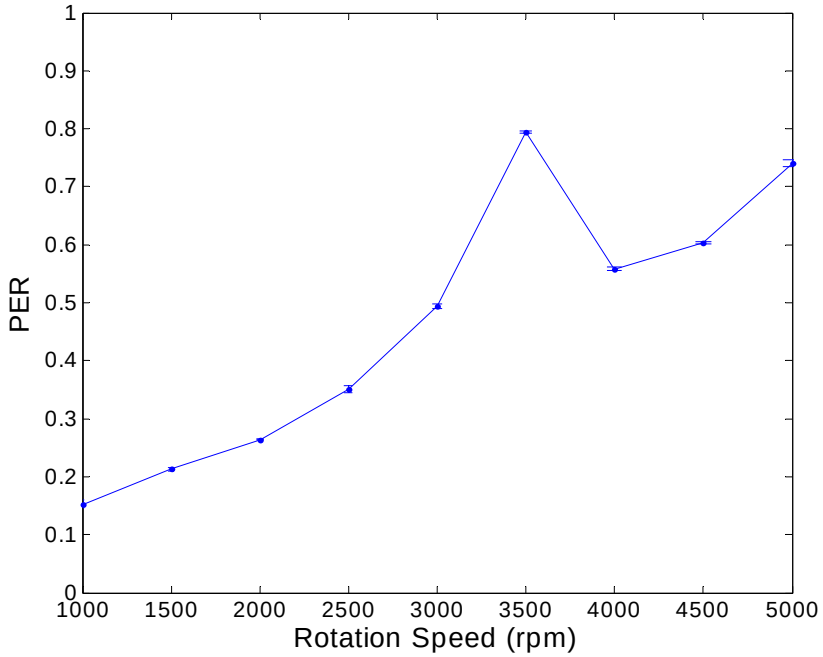

Figure 4.8. PER vs rotation speed .with three evenly spaced 4 degree error regions

4.3.2 Numerical Analysis of First Transmission Error Rate

.

First transmission error rate represents the percentage of packets received with errors in their first transmission attempt.

In order to simplify the calculation of the first transmission error rate, the same error system illustrated in Figure 4.5 is considered and the probability of bit error in the

high error region and low error region is considered as 1 and 0 respectively. Also the rotation speed considered for this system is 2000 rpm. As explained in the previous section the packet transmission start position determines its probability of success. The probability of success of a packet transmission can be determined by finding the length of the safe zone. The safe zone probability of success is 1. But as explained in the previous section the safe zone size is also determined by the maximum back off duration Δ and the ACK duration. Hence the probability calculation should also consider these factors.

If a packet transmission starts Δ+CCA+Packet time duration before the error zone, the transmission would end before the error zone as illustrated in Figure 4.9. The duration between CCA+Packet time and Δ+CCA+Packet time has a success probability of ½, this is because a packet transmission starting in this region can choose between 0 or 1 random back-off period and if it chooses 0, it would finish its transmission before the error zone, while if it chooses 1, it would end the transmission in the error zone.

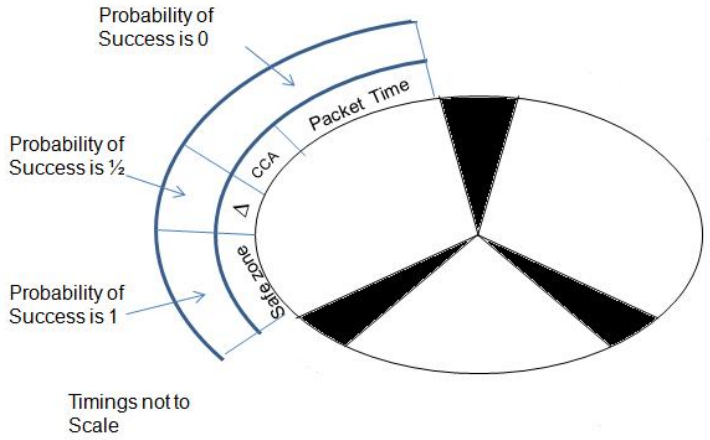

Figure 4.9. Probability of successful packet transmission illustration considering traversed range during CCA, packet time, and random backoff time. While not shown, the same rule applies for the rest of the cycle.

If the sensor position is such that the CCA duration and the random back off duration ensures that the packet transmission starts only after the error zone, the packet is successful. Similar to the above explanation there is a probability of ½ due to the maximum back-off duration Δ. This is shown below in Figure 4.10.

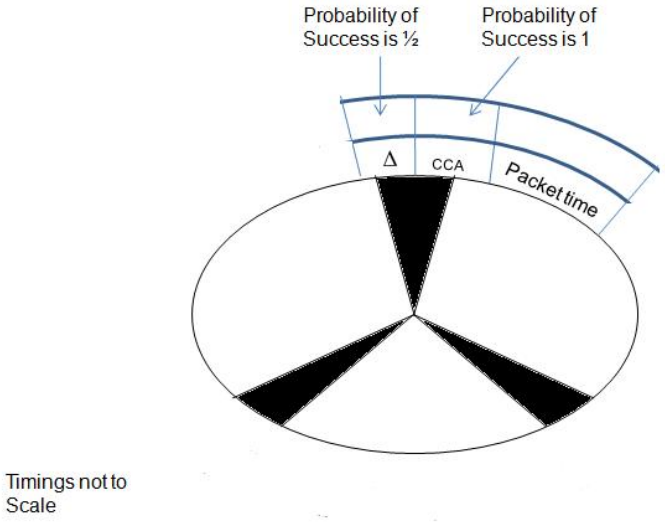

Figure 4.10. Probability of successful packet transmission to miss the error zone, considering traversed range during CCA, packet time, turn-around time, and random backoff time. While not shown, the same rule applies for the rest of the cycle.

Similar analysis applies for successful ACK. Figure 4.11 shows the ACK success regions

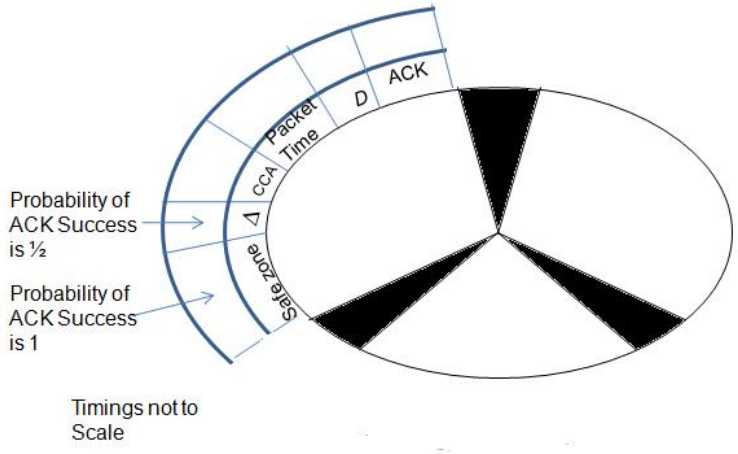

Figure 4.11. Probability of ACK success illustration, considering traversed range during CCA, packet time, turn-around time, and random backoff time. While not shown, the same rule applies for the rest of the cycle.

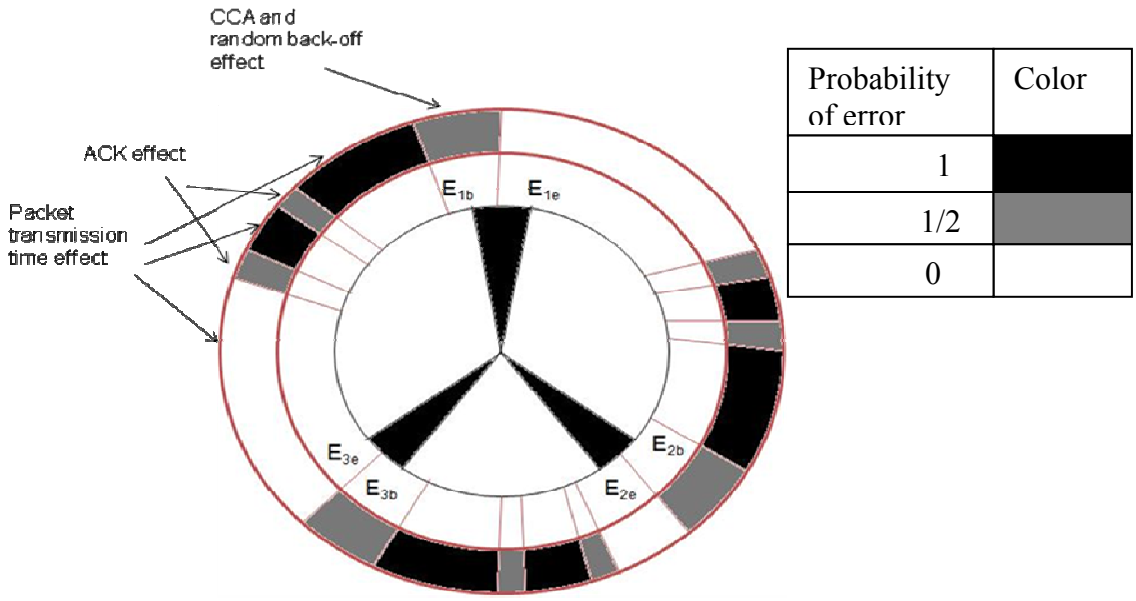

Figure 4.12. First transmission error probability distribution for a three error zone system centered at 0,120 and 240 degrees with width 4 degrees each (E_{1b}=-2º, E_{1e}=2º, E_{2b}=118º,E_{2e}=122º,E_{3b}=238º and E_{3e}=242º).

We derive the probability distribution for a scenario with three error zones centered at 0, 120 and 240 degree each with width 4 degrees. The corresponding probability distribution is shown in Figure 4.12.

The first transmission error rate is given by the equation.

$$\frac{\text{Area under the Red region in Degrees}}{360} \times 1 + \frac{\text{Area under the Grey region in Degrees}}{360} \times \frac{1}{2}$$

To verify the equation simulations are done on the simulator and both the results matched to give the first transmission error rate of 0.37.

The calculation of overall packet error rate which includes the errors in the first, second and other consecutive transmissions is a tedious and complex process. For example the probability of error of the second transmission is a conditional probability depending on the position of the sensor after the end of the first transmission. The overall packet error rate equation will be hard to derive The error rate calculated using conditional probability is for all the possible positions of the sensor and hence can be verified with a simulation which has perfect randomness for all transmissions and retransmission. Achieving this is difficult with the present simulator, so the calculation of the packet error rate is not considered in this thesis.

4.4 Simulation Studies

An error region exists due to the multipath and Doppler effects associated with a specific surrounding, sensor placement and rotation speed. Hence it is expected that the error region distribution changes in different environments. To study the varied transmission error characteristics in a wide range of possible surroundings, a software simulator is developed using C++ to simulate the rotating process, the radio channel properties, and the ARQ transmission method based on any given sensor rotation speed R, the number of error regions and their respective widths and location around the periphery of rotating structure. The simulator keeps track of the instantaneous location of the radio. When a radio transmits a packet, the simulator computes the transmission starting and ending times, and it identifies any segment(s) that are transmitted in an error

region. For each bit transmitted in the error region, a uniform bit error is generated according to a specified bit error probability for each error zone.

The simulator also models the packet transmission and random wait durations precisely according to the IEEE 802.15.4 specification. Each simulation experiment can specify the number of packets to be transmitted, and all packets transmitted are recorded including their received bit contents and timestamps. The simulation also models the ACK transmission time during ARQ transmission.

The simulation is used to study the effect of: i) different error region widths for one error zone, ii) different number of error regions, and iii) imprecise knowledge of the actual rotation speed on the error region distributions, and (iv) a transmission error avoidance scheme. The simulation results shown below are for a constant packet size and considering a probability of bit error of 1 inside the error region and 0 outside the error region. Also the packet generation interval is 0msec.

4.4.1 Effect of Different Error Region Widths

Figure 4.13 shows the error burst distance distribution observed with one error region of different widths. As shown, for one error region, the main modes remained near positions 0 and 1, indicating the consecutive errors occur either at the same location or one spindle periphery distance away, which is again the same location. As the error region width increases, however, a diluting effect to each mode size was observed. This diluting effect is a direct result of the wider range of potential starting times of an error

burst; as a result the width of each mode is proportional to the error region width. The proportional width dilution is observed clearly in Figure 4.13.

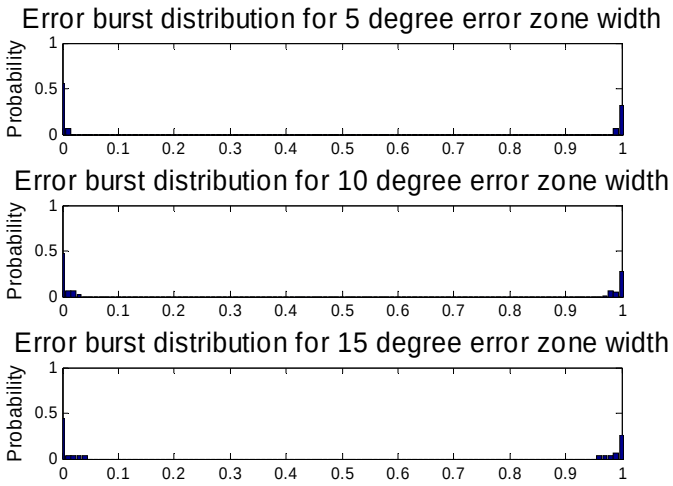

Figure 4.13. Normalized error burst distance distribution obtained with error region widths 5, 10, and 15 degrees at 2000 rpm.

4.4.2 Effect of Different Number of Error Regions

Figure 4.14 shows the error burst distance distribution for one, two, and three evenly distributed error regions each of 4 degrees wide. As clearly shown, the error burst distances correspond to that from an error region to any other regions as well as itself. Hence, the error burst distance distribution graph can be used to estimate the number of error regions in a rotating system if the rotation speed is accurately known.

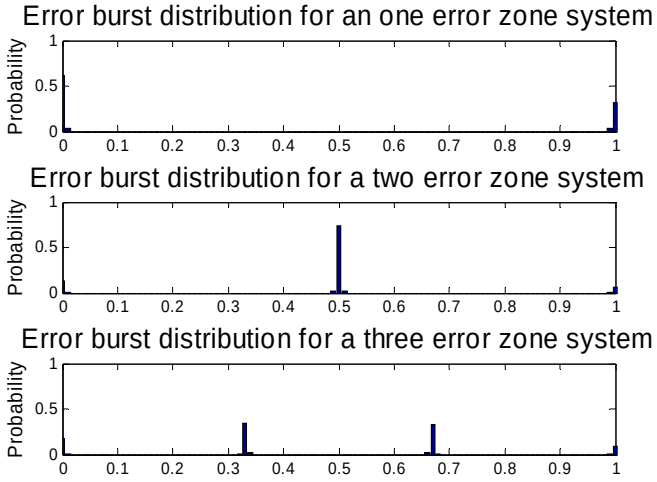

Figure 4.14. Normalized error burst distance distribution for one, two, and three evenly distributed error regions.

4.4.3 Effect of Imprecise Knowledge of Rotation Speed

The error burst distance distribution shown in Figure 4.1 is obtained with a known rotation speed of 2054 rpm. Accurate rotation speed is not, however, always available to either a sensor node or an external operator. This section studies the impact of an imprecise knowledge of the rotation speed on the transmission error pattern. The analysis is conducted by simulating the transmission errors at a rotation speed R rpm while computing the error burst distances based on a potentially imprecise rotation speed of C rpm. The following examines the effects of small inaccuracies that may be caused due to inaccurate speed measurement, as well as the effects of large inaccuracies that may be caused by a total lack of process knowledge. Insights to the latter case are essential for deriving adaptive error pattern discovery methods that can adapt to varying rotation speeds without any knowledge of such speed changes.

Figure 4.15 shows the error burst distance distribution acquired with R=2000 rpm, while C is (a) 50 and 100 rpm lesser than R, and (b) 50 and 100 rpm higher than R. As seen, the inaccurate rotation speed adopted in the error burst distance analysis resulted in various minor modes displaced from the main mode. Such displacements are due to the incorrect assumption of a rotation cycle period. With $C < R$, the sampling period is longer than an accurate period, causing an error burst at the same location to appear relatively earlier during the sampling period. For an error burst that occurs in exactly one true period after the previous error burst, the normalized error distance will be displaced by $\delta = (1/R - 1/C) / (1/C) = C/R\text{-}1$. A negative δ indicates a displacement to the left. If the error burst occurs in exactly k true periods after the previous error burst, the error distance will be displaced by $k(C/R\text{-}1)$. Given the back-to-back transmission pattern in this study, a consecutive error burst mostly occurs in the immediate next cycle, while the probability of more cycles (elapsing prior to a next error) gradually decreases. The finding suggests that a series of equally displaced modes be an indication of a slight inaccuracy in the adopted rotation speed, and the true rotation speed can be found as $R=C/(1+\delta)$.

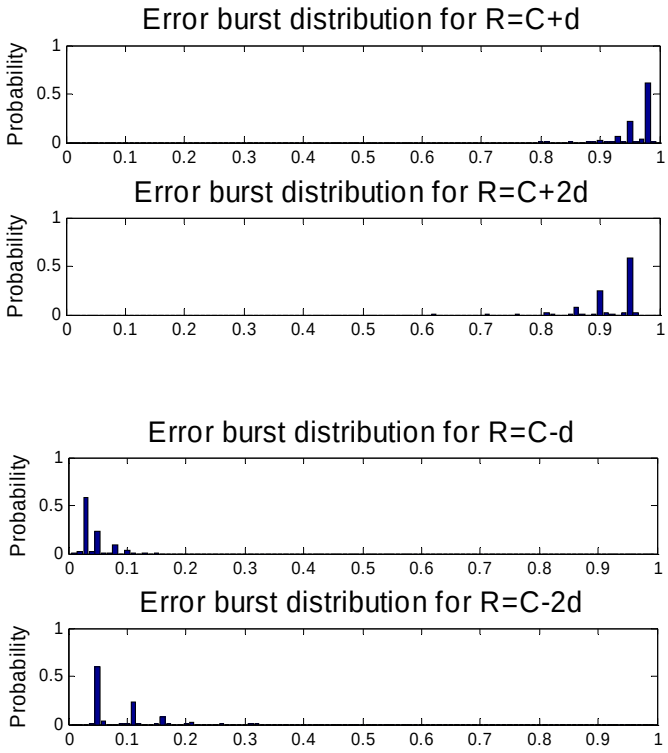

Figure 4.15. Error burst distance distribution obtained for *R*=2000 rpm and (a) *C*=1950 rpm, (b) *C*=1900 rpm, (c) *C*=2050 rpm, (d) *C*=2100 rpm.

Figure 4.16 shows the error burst distance distribution acquired with R = 2000 rpm and $C = R/2$ (1000 rpm) and C=2R (4000 rpm). As seen, the mode displacement expression in the previous section still holds for large speed inaccuracies. With $C=R/2$, the displacement was -0.5; with $C = 2R$, the displacement was 1, which is identical with the original distribution.

Similar displacement expressions are found for scenarios with multiple error regions while the derivations are more complex. For evenly distributed error regions and C integer multiples of the actual rotation speed, the resulting error burst distance distribution can be with the aliasing effect of a sampling process. Consider two error

regions 180 degrees apart. If R=C, the correct distribution is obtained with error burst distances at 0, 0.5, and 1 (Figure 4.17 (a)). With a sampling speed of $C = R/2$, each sampling cycle actually consists of two true cycles; hence, the error burst distribution is expected to consists of two identical distributions in each half of its sampled cycle, as seen in Figure 4.17 (b). With a sampling speed of C=2R, the sampling cycle corresponds to only half of the true cycle; hence, one error region is sampled in each sampling cycle, the other error region is sampled in the next sampling cycle at exactly one sampling cycle later, thus resulting in a distribution identical to that one error region scenario (Figure 4.17 (c)). The figures indicate that the error burst distance distribution can be used to identify errors in the rotation speed and also to determine the error region pattern of the system.

.

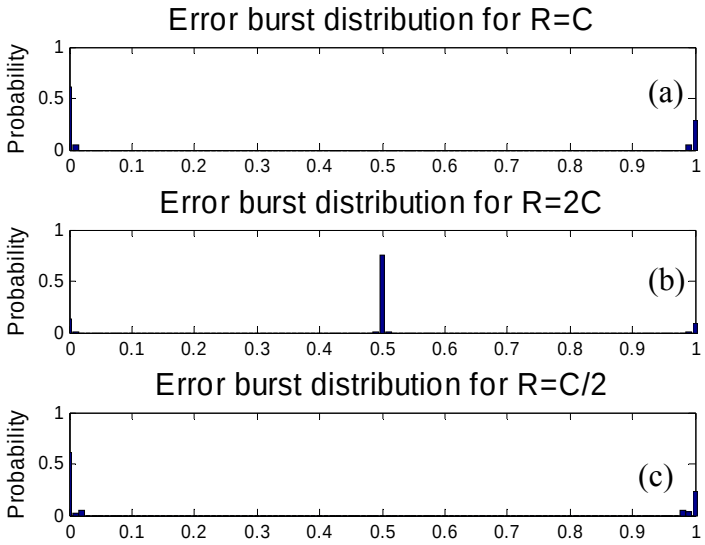

Figure 4.16 Error burst distance distribution for large speed inaccuracies with one error region

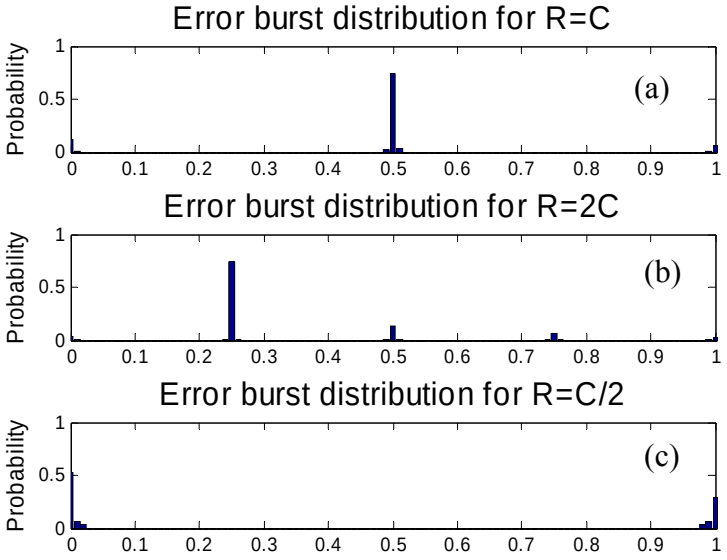

Figure 4.17. Error burst distance distribution for large speed inaccuracies with two error region

CHAPTER FIVE

TRANSMISSION ERROR AVOIDANCE

The purpose of the transmission error avoidance scheme is to enhance the achievable data throughput of a sensor radio by avoiding transmission errors due to rotation.

5.1 Overview of Proposed Method

As explained in previous chapters the knowledge of the error region pattern and its characteristics is important because it indicates the regions of low error probability. To enable error avoidance, the receiver records the time stamps and bit contents of all packets received with errors; the error distribution is then analyzed and the transmitting radio is informed to control its packet transmission time. The error transmission scheme should include measures to overcome the effects of imprecise knowledge of the rotation speed and the sensor clock drift. Another problem is the transmitting sensor has to be synchronized to the error pattern. Our scheme takes all these factors into consideration and consists of two different phases: the error identification phase and the operational phase.

The error identification phase involves determining the error region distribution. The purpose of obtaining an error region distribution is to identify the low *or zero BER* regions within each rotation cycle for data transmission. Given the assumption that a sensor does not know its position at a point of time, it relies on the transmission success

and failure events to infer whether it is inside or outside an error region each time it transmits.

The error burst distance distribution discussed in Section 4.1 does not convey the actual number of error regions or the location of such regions. Figure 5.1 shows the close similarity between the simulated error burst distance distributions for two different error region distributions. The three error zone system with error regions centered at 0, 90 and 180 degrees has a similar error burst distribution to a four error zone with error regions centered at 0, 90,180 and 270 degrees. This makes it hard to distinguish between an asymmetric three error zone system from a symmetric four error zone system by studying the error burst distribution. This calls for the use of *error burst location distribution*. The error burst location distribution is discussed below.

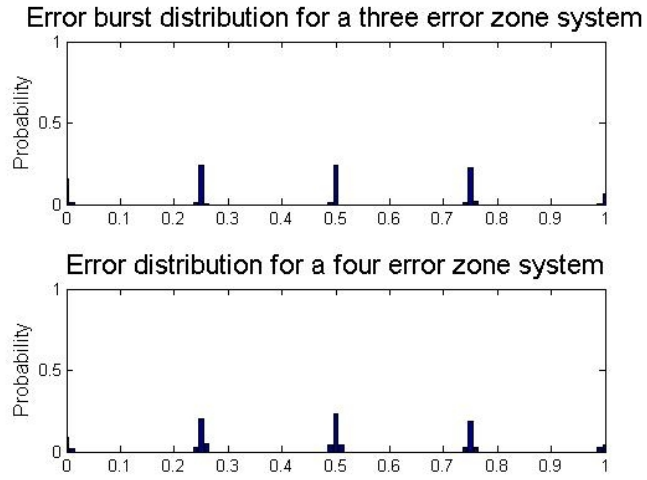

Figure 5.1. Two error region distributions can result in similar error burst distance distributions: (a) three error regions centered at 0, 90, and 180 degrees; (b) four error regions centered at 0, 90, 180, 270 degrees.

Definition 2: Error Burst Location Distribution

Given the beginning timestamps of a set of N consecutive error bursts, let the *normalized distance* between the i^{th} and i+1^{th} error bursts be D_i and T_R the duration for one revolution of the spindle, the first error burst's beginning location as the reference origin, the normalized error burst location for the i^{th} error burst is defined as

$$L_i = \left(\sum_{j=1}^{i} D_{j-1} \right) \bmod T_R \tag{3}$$

Sensor clock drift is the main challenge when obtaining the location distribution. Clock drift renders the recorded timestamps and calculated error burst locations to drift from their actual location. In fact, this was the main reason that error burst distance distribution discussed in Section 4.1 was used initially to find discernible error regions instead of using location distribution. As the machine does not provide digital clock output, a visual assessment found the sensor clock to lead approximately 15 seconds ahead the machine clock every 12 minutes. Fig. 5.2 shows the location distribution subject to clock drift.

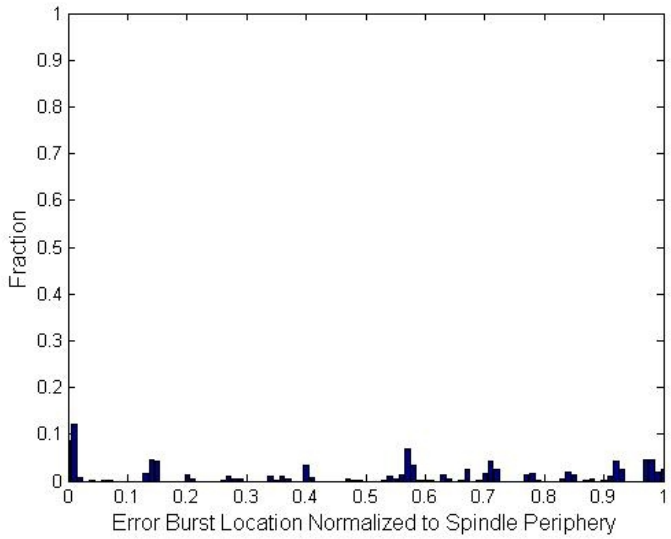

Figure 5.2. Location distribution with clock drift for error bursts shown in Figure 4.1.

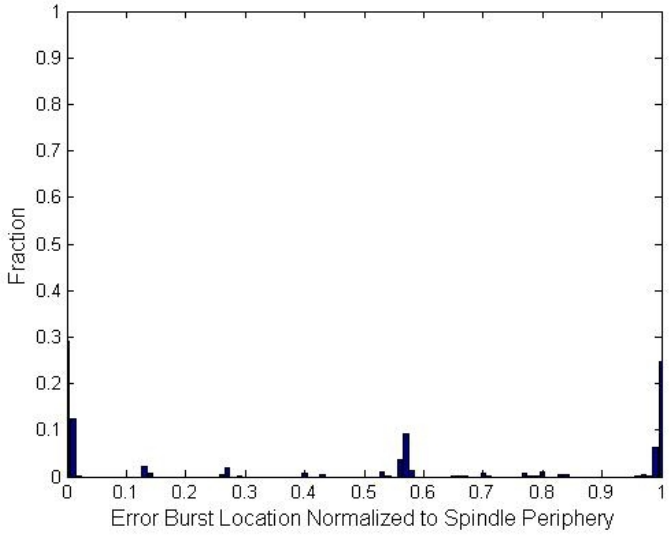

Figure 5.3. Calibrated error burst location distribution.

To compensate for the drift impact, accumulated error in the estimated error burst locations must be calibrated periodically. Without external synchronization, the calibration is done by analyzing the location distribution in small time windows and aligning the resulting distributions. Fig. 5.3 shows the calibrated location distribution derived by analyzing and aligning the location distribution for every 10 error bursts. The calibrated error burst location distribution clearly indicates the error regions in the system.

The error burst location distribution shown in Figure 5.4 corresponds to a system with three error zones centered at 0, 90 and 180 degrees, each with a width of 4 degrees. The error burst location distribution is assumed to be generated with the correct rotation speed and the effects of the sensor clock drift is not considered. This figure when compared to Figure 5.1(a) itself shows the effectiveness of using the error location distribution because it clearly indicate the asymmetric nature of the system, while the error burst distance distribution indicates a symmetric system The error zones are identified by determining the bins of the error location distribution with a probability of bit error greater than a particular threshold. The width of the error zone depends on the resolution of the bins of the error burst location distribution. Figure 5.4 has a resolution of 3.6 degrees, so each bar in the histogram corresponds to 3.6 degrees. The position of the error zone is always found relative to the first error burst is shown in the figure. Therefore the error burst distribution indicates error locations at 0, 0.25 and 0.5 (in terms of spindle periphery) distance away from the first error seen.

If the correct rotation speed is not used in generating the error burst location distribution, it would not be possible to identify the error regions as discussed in Section 4.4. Figure 5.5 shows the percentage difference between the error burst location distribution generated with a rotation speed of 2054 rpm and the error burst location distribution generated with a rotation speed of 2000 rpm. The percentage difference is large even after many probe packets are used in generating the location distribution. Thus the error identification phase should begin with a phase to identify the correct rotation speed before generating the error burst location distribution.

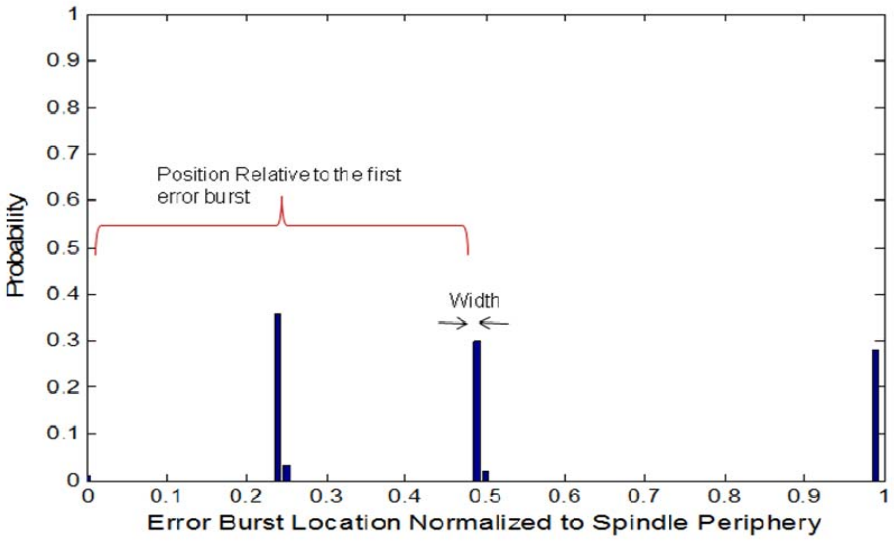

Figure 5.4. Error burst location distribution for a three error zone system centered at 0,90 and 180 degrees, each with a width of 4 degrees.

Another factor considered is the number of probe packets to be sent before which it can be concluded that the error location distribution is an accurate representation of the error properties of the system. Figure 5.6 shows the percentage error in the error location

distribution with the number of probe packets. So with more probe packets the error location distribution becomes more accurate. The steps involved in the error identification phase are explained in the next section.

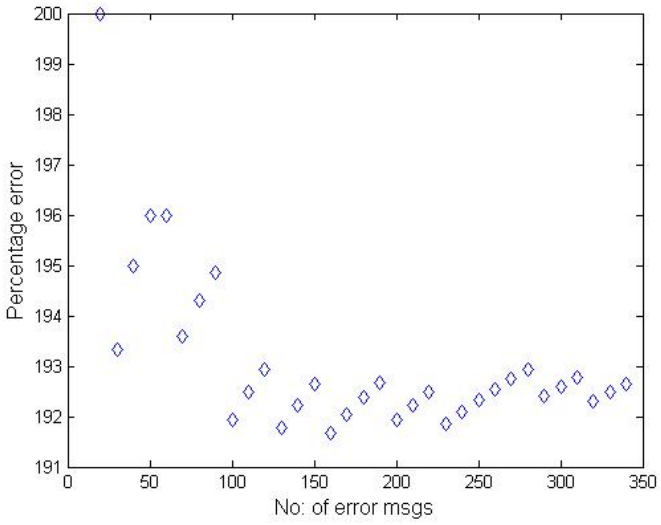

Figure 5.5. Percentage error in error location histogram if the rotation speed is considered as 2054 rpm when the actual rotations speed is 2000rpm, vs number of probe packets with error

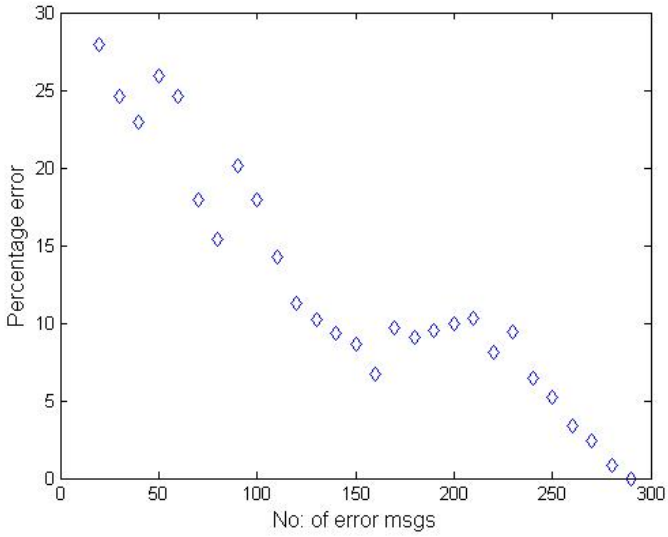

Figure 5.6. Percentage error in error location histogram vs number of probe packets with error

In the operational phase, the sensor begins with data transmission. Initially, transmissions can occur at any time when data are present until a number of transmissions are received with errors in a predefined time window. The sensor analyzes the error packets' timestamps to logically deduce its present location with respect to (i.e. synchronize with) its error burst location distribution. Once it successfully synchronizes, it starts to control the times of its data transmissions. Prior to each transmission, the expected transmission interval is estimated based on the IEEE 802.15.4 medium access control procedure and parameters; a data transmission is permissible when its expected duration does not overlap with any error region; otherwise, the transmission will be delayed until the end of an earliest error region with a following low-error duration that is sufficient for the transmission to complete.

To determine the exact time an error burst occurs within an arbitrary data packet carrying real application payload is more difficult than that with probing transmissions. Since the data contents are not known previously, the location where bit errors have occurred cannot be directly determined. There are methods to explore this information without substantial overheads. For example, since ARQ is adopted, packets are retransmitted until they complete successfully. By caching and comparing packets in error with their successful retransmissions, the error burst times can be found. For another example, transmitted data can be encoded with known bit patterns at predictable intervals in each packet, then error burst times in each packet can be identified at a granularity proportional to the encoding interval. These approaches are not considered in this thesis.

The purpose for an error avoidance approach is to improve energy efficiency and data throughput. It is beneficial when the following conditions are satisfied

1. The PER for unconstrained transmissions is found to be unacceptably high
2. Error region distribution obtained in the error identification phase reveals distinguishable error regions
3. Intervals between identified error regions have much lower PER and are long enough to complete at least one data transmission

The proposed error avoidance scheme works by avoiding high error regions and if no high error regions are identified for a system, then there would be no purpose in implementing the error avoidance approach as there would not be any improvement in the throughput. Unless there are low PER regions in between the high error regions there

would be no improvement in throughput. The packet size duration should also be lesser than the interval between identified error regions or else the throughput would be less. This case is illustrated in the simulation results section.

5.2 Error Identification Phase

In the error identification phase, the sensor uses probing transmissions to collect sufficient transmission history to establish the error burst location distribution. The sensor needs to first make sure that the generated error location distribution is correct. For this it should first make sure that the assumed rotation speed of the spindle is correct. It can make use of the error burst distribution to find out the error due to the imprecise knowledge of the rotation speed as discussed in section 4.3.3. This would require a sampling speed varying algorithm which is not discussed in this thesis and the rotation speed is assumed to be correct in the simulations. The sensor should then generate the calibrated error location distribution which is devoid of sensor clock drift errors. Given the distribution, the center and width of each error region with PER above a chosen threshold is identified. In section 4.2, it was shown that the error region width depends on the assumed BER for the error region. The higher the assumed BER, the narrower the width, while the more chances an error could occur outside the defined error region. Probing packets are transmitted and analyzed until the percentage change in the error location distribution is below a specified threshold. Figure 5.6 and section 5.1 discusses the percentage change in the error location distribution with the number of probing

packets, but further discussions on the choice of threshold is not studied in this thesis. At the end of the error identification phase the number of error regions, the center and width of each error region is known.

5.3 Operational Phase

The phases involved in the operational phase are given below.

5.3.1 Synchronization

In the operational phase, the receiver first synchronizes with a given error burst location distribution by observing the timing of multiple error bursts, it then proceeds with transmission time control.

The pseudo code for synchronization is shown in Figure 5.7.At any given time if the transmitting sensor wants to synchronize with the error regions, it requests the latest N consecutive error burst's burst distance sequence $\{D_i\}$, the error burst location $\{L_i\}$, the first error burst's time stamp t_0 and the receivers current time t_nowrx. It also records its current time t_nowtx. Using the error burst distribution it checks the error burst location distribution L_i which it is closest to below a threshold E as shown in Figure 5.7. Once synchronization is complete the transmitter can determine its location $C_{Tx}(t\_now_{Tx})$ as $L_i + (t\_now_{Rx} - t_0)$ * rotation speed.

```
{Di}: error burst distances for N consecutive error bursts
{Lj}: error burst location distribution
M: number of identified error regions
δ: error region width
E: miss rate threshold
C: current location
s: miss count
i: error burst index
 START
for j=1 to M
        C= Lj, s=0, i=1, k=j;
        while (i<N)
                if( (C+Di) ∈ Lk+1±δ)
                        C= Lk+1, k=k+1;
                else
                        C=C+Di, s=s+1;
                endif
                i=i+1;
        end while
        if (s/N)<=E
                Synchronization Complete;
                Break;
        endif
end for
```

Figure 5.7. Synchronization algorithm

Once the synchronization completes successfully, the receiver informs the transmitting sensor of the last error burst timestamp and its corresponding synchronized location C_{TX}. If the algorithm ends unsuccessfully, the algorithm must be repeated at a later time.

5.3.2 Transmission Error Avoidance

Assuming the transmitting sensor and the receiver have synchronized local clocks, the transmitting sensor can determine at any time, its location and the duration until beginning of the next error region. It also can determine the end of the nearest following error region with a low-error region no shorter than the estimated transmission time of the next packet. The transmitting sensor can then go on to schedule its transmission to avoid the error regions.

The IEEE 802.15.4 MAC protocol version considered for implementing the transmission error avoidance scheme is the non-beacon mode version. Before any packet transmission the radio waits for a clear channel access (CCA) duration and a random number of back-off slots τ (section 3.2). The standard allows setting minimum values for the random backoff parameters to limit the minimum backoff window to 2^0 backoff period which is considered for the proposed transmission scheme Hence the maximum number of back-off slots Δ, before packet transmission is 1.

The error avoidance algorithm shown in Figure 5.8 calculates the delay that needs to be injected before scheduling a packet transmission to avoid the error region. The algorithm is run before every packet is sent out. Before every transmission the algorithm checks if the CCA+Δ+Packet time duration will result in the transmission ending in the error zone. If this is the case then the packet transmission is scheduled to start only after the error region. If the separation between the error zones is not large enough for a packet transmission the transmission is further delayed to start only after the second error zone.

```
{L_j}: error region locations
M: number of identified error regions
δ: error region width
P: packet transmission duration
C: current sensor location
CCA: CCA duration
Δ: maximum back-off slot
START
for j=1 to M
        if( ( (C+P+CCA+Δ) ∈ L_k±δ ) || ( ( (C+CCA)< L_k-δ) &&
        ( (C+CCA+P)> L_k+δ) ) )
                if(P>( L_k+1- L_k) )
                        C= L_k+1+δ-CCA;
                else
                        C= L_k+δ-CCA;
                endif
        endif
        i=i+1;
end for
```

Figure 5.8. Error avoidance algorithm

5.4 Simulation Results

The rotating wireless sensor simulator explained in section 4.3 is used to verify the effectiveness of the transmission error avoidance scheme. The error regions are assumed to be identified and the error identification phase is assumed to be successful. The radios are also assumed to have synchronized with the error distribution. The IEEE 802.15.4 non-beacon mode data and ACK transmission timing is modeled. Table 5.1 summarizes the simulation parameters.

Table 5.1. Simulation parameters

Parameter	Value
Radio link rate	250 kbps
Radio symbol duration	16 usec
CCA duration	8 symbols
Radio turn-around time	12 symbols
ACK frame	22 symbols
ACK timeout	2.4 msec (sensor default [11])
Spindle rotation speed	2000 rpm
Backoff slot duration	20 symbols

The simulations are done to verify the advantages of the transmission error avoidance scheme mainly the packet error rate and throughput improvement. The effect of the number of error regions on the performance of the error avoidance scheme requires testing. To do so, simulations are done on a one error zone symmetric system and a four error zone symmetric system. The bit error rate inside the error zone is considered as 100% and outside the error zone as 0%. In reality the bit error rates inside the error zone would be less than 100% and outside the error zone would be greater than 0%. The effect of such a scenario is also studied. Lastly the performance in an asymmetric two error zone system is studied to understand the importance of the packet size in the error avoidance scheme. The results of the simulations are discussed below.

100 % BER Inside Error Region, 0% BER Outside Error Region

This is an idealized setting that illustrates the typical benefit of the scheme. Figure 5.9 shows the PER and data throughput achieved when there was one error region (4 degree wide) with and without error avoidance, with different packet sizes and packet generation intervals. A 0-second interval represents saturating transmission at the link's maximum capacity. In Figure. 5.9(a), it is seen that larger packets had higher PERs on average; PERs remained consistent with different packet generation intervals, reaching about 10% with 92 byte packets.

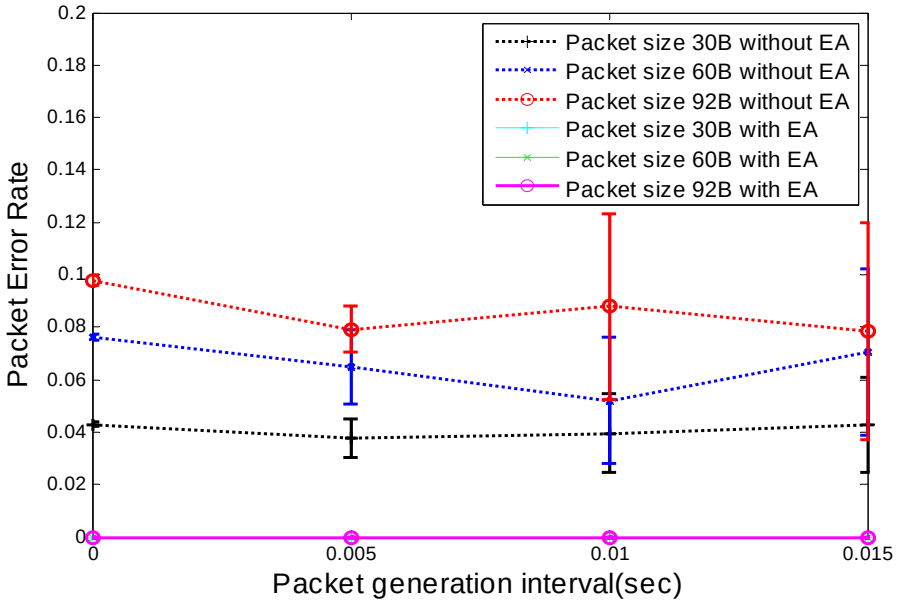

(a)

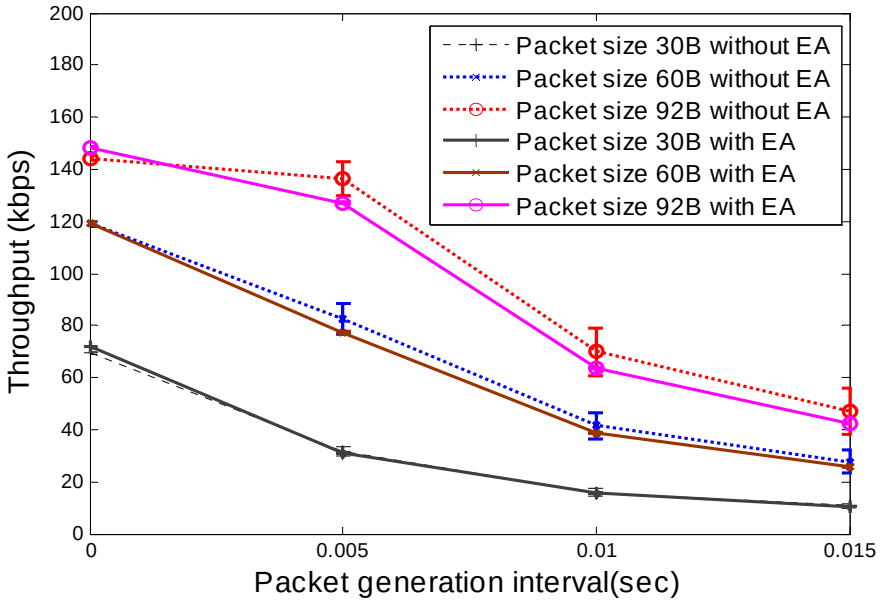

(b)

Figure 5.9. 2000rpm, one 4-degree error region, (a) PER v.s. packet size v.s. transmission interval (b) throughput v.s. packet size v.s. packet interval.

With error avoidance, errors were completely avoided, while a slight decrease in throughput was seen.

A more challenging scenario was studied with four error regions each 4 degree wide and centered at 0, 90, 180, and 270 degrees. Figure 5.10 shows the PER and Figure 5.11 shows the throughput. Interestingly, with scattered error regions, PERs increase as packets are generated faster, reaching 50% with 92 byte packets. With error avoidance, throughputs were substantially increased (50 to75% for continuous transmissions). Also interesting was that with- and without-error-avoidance throughput curves came close as the packet interval increased; they merged eventually, and the merging point depended on the packet sizes – the larger the size, the later the merge, the more throughput gain achievable with error avoidance.

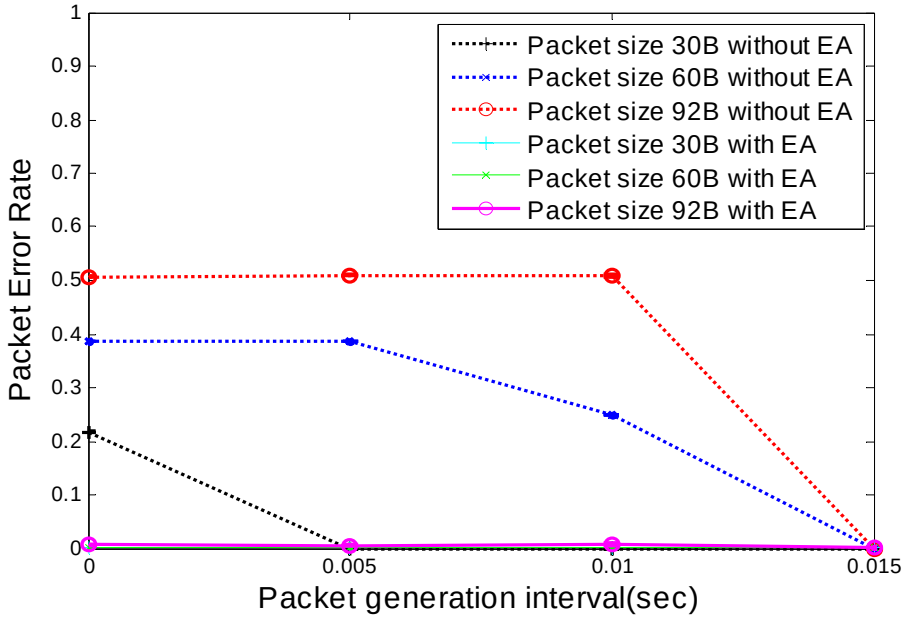

Figure 5.10. 2000rpm, four 4-degree error regions PER v.s. packet size v.s. transmission interval

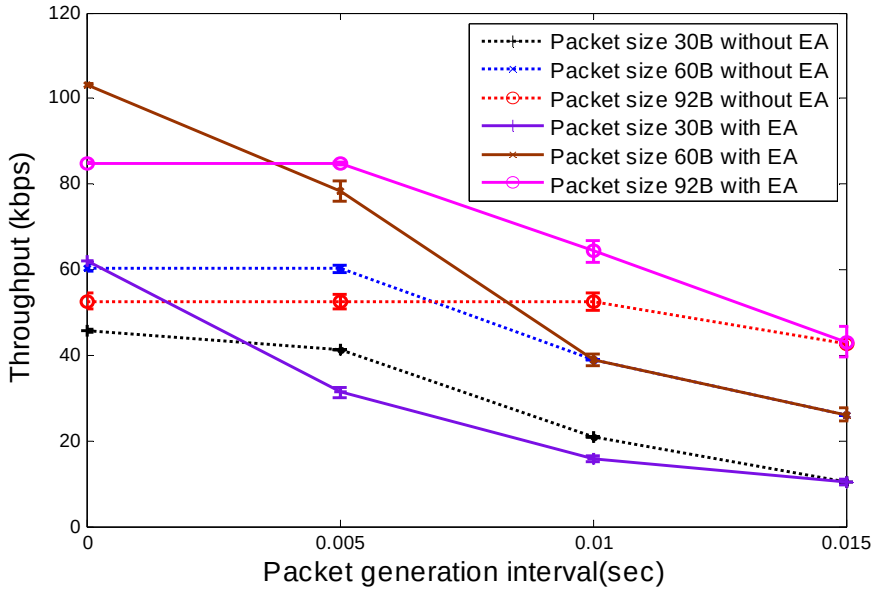

Figure 5.11. 2000rpm, four 4-degree error regions Throughput v.s. packet size v.s. transmission interval

Less than 100 % BER Inside the Error Region, non Zero BER Outside the Error Region

In practice, BERs inside and outside error regions may not be 100% and 0%. Figure 5.12 shows the achieved throughput with different BERs outside the error region. When BERs were 0.01 or less, error avoidance increased achievable throughput by nearly 40% when data rate is very high. Once the BER approached 0.1, substantial errors occurred even outside the error region therefore error avoidance was no longer beneficial. The BERs at different levels of magnitude were chosen to represent a wide range of typical environments.

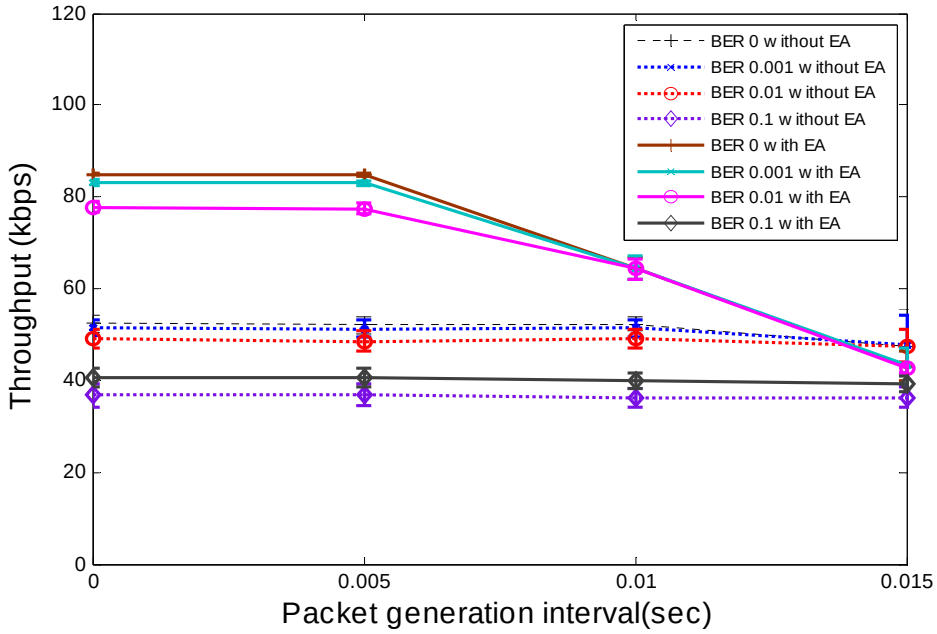

Figure 5.12. 2000rpm, four 4-degree error regions, throughput v.s. PER outside error region with 92 byte packets (BER in error region is irrelevant since transmissions are entirely avoided).

Packet Size Relationship with Error Region Separation

A two error system with error regions centered at 0 and 60 degree, each with a 4 degree width is considered, the BER inside the error region is 1 while the BER outside the error region is 0. The throughput for different packet sizes at different packet generation intervals with error avoidance is analyzed. Figure 5.13 shows the result. The distance between the error regions corresponds to the transmission duration of a 150 byte packet. So for any packet size above 150 bytes the two error regions are considered as one error region by the transmission avoidance scheme and hence the throughput decreases with the increase in packet size. This result can be used in deciding the packet size for transmission. Another factor which is seen is that the packet generation interval doesn't have an effect on the throughput for larger packet sizes. This is because the packet transmission interval itself would be smaller than the packet transmission duration hence resulting in a constant throughput for different packet generation intervals.

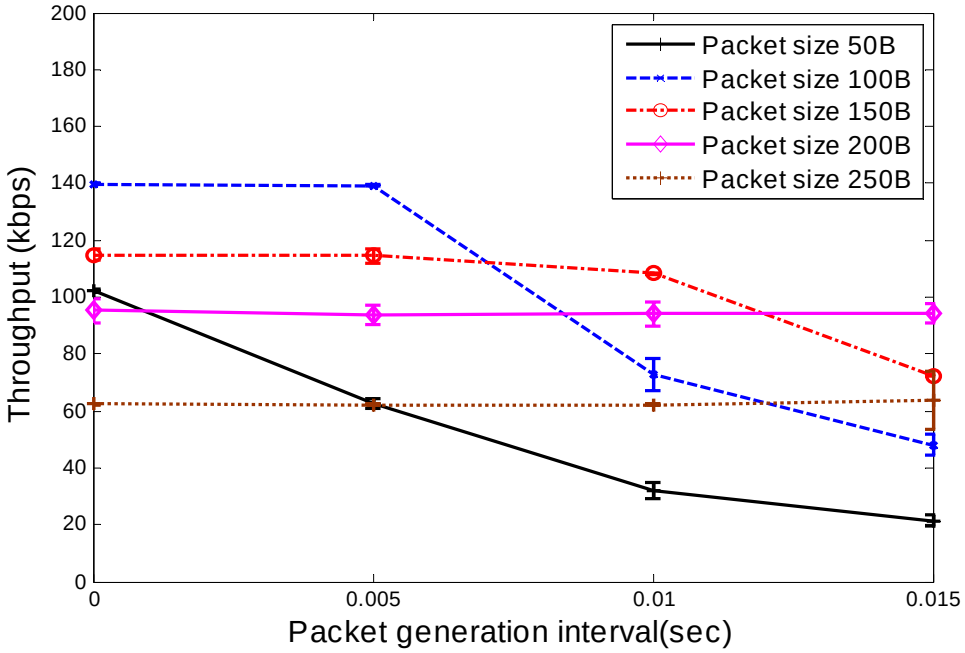

Figure 5.13. 2000rpm, two 4-degree error regions centered at 0 and 60 degrees, throughput v.s. packet size for different packet generation interval.

CHAPTER SIX

CONCLUSIONS AND FUTURE WORK

6.1 Conclusions

The thesis utilized a rotating machine testbed as well as a software simulator to investigate the transmission error patterns experienced by a wireless sensor mounted on a fast rotating structure. A model for transmission error patterns is developed through analysis of packet transmissions in a testbed. The model is used for on-line error pattern identification, communication performance prediction, and development of intelligent error-avoidant transmission methods.

From the testbed experiments it is found that:

- One specific error region on the spindle periphery is identified by analyzing the transmitted packets' normalized error burst distance distribution,
- The width of the error region is estimated using a sliding window algorithm with a range of different packet error rates, and
- The normalized error burst distance distribution sensitively depends on the accurate knowledge of the true rotation speed.

From the simulation experiments it is found that:

- The larger width of an error region led to a dilution of each mode in the error burst distance distribution,

- From an error burst distance distribution the number of distinct error regions can be estimated,
- Discrepancy between the true rotation speed and the speed adopted by the error burst distance analysis resulted in a series of aliasing modes, and displacement between such modes can be used to assess the speed discrepancy, and
- With multiple error regions, the speed discrepancy can be similarly identified by analyzing the aliasing effects.
- It was shown that a relatively small region with disadvantaged radio propagation can cause substantial errors and energy wasted in retransmissions.

In this thesis the PER is analytically shown to have a generally increasing trend with increasing rotation speeds, while exceptions can occur at certain speeds depending on the error region distribution if the ACK option is enabled. Numerical analysis was also able to predict the first transmission rate accurately for a given error system.

This thesis also proposes an online error inference and error-avoidance transmission method for sensors with low accuracy clocks. With simulation, the method was shown to be particularly effective when required data transmission rates are high and error regions are scattered around the periphery. For a one error zone system with an error region width of four degree, the packet error rate was reduced to 0 with transmission error avoidance. A four error zone symmetrical system with error region widths 4 degree shows 50% reduction in packet error rate with a 75% improvement in throughput. The packet size also affects the data transmission throughput. Larger the

packet size, lesser would be the throughput for an asymmetrical two error zone system with error width 4 degrees.

6.2 Future Work

The first phase of the error avoidance scheme is the error identification phase. The effects of imprecise knowledge of rotation speed and the effects of clock drift on the error burst distribution are shown. It was shown in Section 4.4 that by changing the sampling speed and analyzing the error burst distribution, the correct rotation speed can be determined. Such a rotation speed aware algorithm needs to be incorporated into the error identification phase to determine the correct rotation speed.

It was also shown in Section 5.1 that calibration of the error burst location distribution is required to avoid the clock drift errors. This calibration algorithm needs to be incorporated and verified for different scenarios. Also the synchronization algorithm in the presence of clock drift and rotation speed error needs to be verified.

The present simulator can simulate the error characteristics of up to four error zones. A more generalized simulation to generate the error characteristics for any number of error zones needs to be developed.

REFERENCES

[1] Akyildiz, I. F., Su, W., Sankarasubramaniam, Y., and Cayirci, E., "Wireless Sensor Networks: A Survey,"Computer Networks 38(4), 393-422 (2002)

[2] Straser, E. G., [A Modular, Wireless Damage Monitoring System for Structures], Ph.D. Thesis, Stanford University, Stanford CA (1998).

[3] Miettien, J., Salemenpera, P., Jarvinen, V., and Hervonen, M., "Wireless Operation Monitoring System for Polymer Covered Cylinders in Rolling Contact*," in Proceedings of the ASME Engineering Technology Conference on Energy*, Petroleum Division 2, 1019-1023 (2002).

[4] Varghese, B., Pathare, S., Gao, R., and Guo, C., "In-process Monitoring of Truing Using a Sensor Integrated Diamond Grinding Wheel," *Transactions of NAMRI/SME 30*, 295-302 (2002).

[5] Dzapo, H., Stare, Z., and Bobanac, N., "Portable Wireless Measuring System for Monitoring Motor Shaft Parameters," *in Proceedings of the Instrumentation and Measurement Technology Conference*, 901-906 (2004).

[6] Sarkimaki, V., Tiaien, R., Lindh, T., and Ahola, J., "Applicability of ZigBee Technology to Electric Motor Rotor Measurements," *in Proceedings of the International Symposium on Power Electronics Electrical Drives Automation and Motion*, 1-5 (2006).

[7] Sundararajan, V., Redfern, A., Schneider, M., Wright, P., and Evans, J., "Wireless Sensor Networks for Machinery Monitoring," *in Proceedings of the International Mechanical Engineering Congress and Exposition*, 1-9 (2005).

[8] Werb, J., Newman, M., Berry, V., Lamb, S., Sexton, D., and Lapinski, M., "Improved Quality of Service in IEEE 802.15.4 Mesh Networks," *in Proceedings of the International Workshop on Wireless and Industrial Automation*, 1-6 (2005).

[9] Ota, N., and Wright, P., "Trends in Wireless Sensor Networks for Manufacturing," *International Journal of Manufacturing Research 1(1)*, 3-17 (2006).

[10] Tang, L., Wang, K.-C., Huang, Y., and Gu, F., "Channel Characterization and Link Quality Assessment of IEEE 802.15.4-Compliant Radio for Factory Environments," *IEEE Transactions on Industrial Informatics 3(2)*, 99-110 (2007).

[11] Wang, K.-C., Tang, L., and Huang, Y., "Wireless Sensors on Rotating Structures: Performance Evaluation and Radio Link Characterization," *in Proceedings of the WinTECH Workshop at ACM MobiCom*, 3-10 (2007).

[12] Tang, L., Wang, K.-C., and Huang, Y., "Performance Evaluation and Reliable Implementation of Data Transmission for Wireless Sensors on Rotating Mechanical Structures," *Structural Health Monitoring*, accepted (2008).

[13] Wang, K.-C., Jacob, J., Tang, L., Huang, Y., and Gu, F., "Error Pattern Analysis for Data Transmission of Wireless Sensors on Rotating Industrial Structures," *in Proceedings of SPIE*, vol. 6932, 2008.

[14] Wang, K.-C., Jacob, J., Tang, L., and Huang, Y., "Transmission Error Avoidance for IEEE 802.15.4 Wireless Sensors on Rotating Structures," *in Proceedings of ICCCN 2008*.

[15] IEEE, [IEEE Standard 802 Part 15.4: Wireless Medium Access Control (MAC) and Physical Layer (PHY) Specifications for Low-Rate Wireless Personal Area Networks] (2003).

[16] Zhao , J., Govindan, R., "Understanding packet delivery performance in dense wireless sensor networks," *in Proceedings of 1st ACM Conf. Embedded Network Sensor Systems,* 1–13(2003)

[17] Lal, D., Manjeshwar, A., Herrmann, F., Uysal-Biyikoglu. E., Keshavarzian, A.,"Measurement and characterization of link quality metrics in energy constrained wireless sensor networks," *in Proceedings of Globecom*,446–452(2003)

[18] Ganesan, D., Krishnamachari,B., Woo, A., Culler, D., Estrin, D., Wicker, S., "Complex Behaviour at Scale: An Experimental Study of Low-Power Wireless Sensor Networks", UCLA, Tech. Rep. CSD-TR 02-0013, 1–11(2003).

[19] Srinivasan, K, Levis, P., "RSSI is under appreciated," *in Proceedings of. 3rd Workshop on Embedded Networked Sensors,* 1–5(2006).

[20] Valente, A., Morais, R., Serodio, C., Mestre, P., Pinto, S., Cabral, M. "A ZigBee Sensor Element for Distributed Monitoring of Soil Parameters in Environmental Monitoring," *in Proceedings of IEEE Sensors,* 135-138 (2007)

[21] Cho, H., Jung, Y., Choi, H, Jang, H., Son, S., Baek, Y., "Real Time Locating System for Wireless Networks using IEEE 802.15.4 Radio, " *in Proceedings of SECON* , 578-580 (2008)

[22] Hara, S., Zhao, D., Yanagihara, K.; Taketsugu, J.; Fukui, K., Fukunaga, S., Kitayama, K., "Propagation characteristics of IEEE 802.15.4 radio signal and their application for location estimation", *in Proceedings of Vehicular Technology Conference*, 97 – 101 (2005).

[23] Hui, Jonathan W., Culler., David E."Extending IP to Low-Power, Wireless Personal Area Networks". Internet Computing 12(4), 37 – 45(2008)

[24] Rappaport, T. S., [Wireless Communication – Principles and Practice], 2nd Ed., Prentice Hall, New Jersey (1996).

[25] Chiasserini, C-F. , and Garetto, M., "An Analytical Model for Wireless Sensor Networks with Sleeping Nodes," Transactions on Mobile Computing 5(12), 1706-1718(2006).

[26] Crossbow Technology, Inc., http://www.xbow.com, accessed April 2007 (2007).

[27] CC2420 data sheet, http://www.chipcon.com/files/CC2420_Data_Sheet_1_3.pdf, accessed April 2007 (2007).